IEEE Access
Multidisciplinary ⋮ Rapid Review ⋮ Open Access Journal

Received 21 February 2024, accepted 29 February 2024, date of publication 4 March 2024, date of current version 8 March 2024.

Digital Object Identifier 10.1109/ACCESS.2024.3373189

RESEARCH ARTICLE

Coordinated Planning of Electricity-Hydrogen Integrated Energy System Considering Lifecycle Carbon Emissions

HAIHONG BIAN[1], CHENGANG ZHOU[1], ZHENGYANG GUO[2], YIZHOU ZHOU[3], (Member, IEEE), AND QUANCE REN[1]

[1]School of Electrical Power Engineering, Nanjing Institute of Technology, Nanjing 211167, China
[2]Hangzhou Power Supply Company of State Grid Zhejiang Electricity Power Company Ltd., Hangzhou 310016, China
[3]College of Energy and Electrical Engineering, Hohai University, Nanjing 210098, China

Corresponding author: Chengang Zhou (1005188889@qq.com)

This work was supported in part by the Graduate Science and Technology Innovation Fund Project TB202317076.

ABSTRACT Hydrogen energy is a promising solution to reaching carbon emissions peak and carbon neutrality. With the development of hydrogen energy devices, coupling hydrogen energy with renewable energy for power generation can compensate for the intermittency and instability of renewable energy. Furthermore, the two-stage coordinated planning of integrated energy system (IES) and electricity-hydrogen integrated energy system (EHIES), compared to independent planning, can help generate additional benefits and reduce carbon emissions. Therefore, this paper proposes a coordinated planning of EHIES considering lifecycle carbon emissions. In the first stage, aiming to minimize investment costs, network losses, voltage deviations, and lifecycle carbon emissions, the equipment capacity and location of EHIES is determined. The life cycle assessment (LCA) method is used to quantify the lifecycle carbon emissions of the EHIES, preparing for the coordinated operation in the second stage. Subsequently, in the second stage, using carbon emissions flow to allocate users' responsibility for emissions, the carbon emissions per unit electricity of the IES system are calculated. With the optimal cost of independent operation for IES and EHIES as the coordinated operation objective, the alternating direction method of multipliers (ADMM) is employed for sequential solution, obtaining the carbon emissions reduction amount, and iteratively updating until convergence. Finally, the effectiveness of the proposed method is verified by using the IEEE 33-bus power distribution network (PDN) and natural gas 6 node systems. The results show that compared to independent planning, the two-stage coordinated planning method reduces the overall operating cost of IES by 3.81% and decreases carbon emissions by 15.89%. This method is effective in reducing the carbon emissions of IES.

INDEX TERMS ADMM, two-stage coordinated planning model, electricity-hydrogen integrated energy system, lifecycle carbon emissions.

NOMENCLATURE

ACRONYMS

ADMM	Alternating direction method of multipliers.
DES	Distributed energy system.
EHIES	Electricity-hydrogen integrated energy system.
ESS	Electric storage systems.
EV	Electric vehicles.
FC	Fuel cells.
FCS	Fast-charging station.
GB	Gas boiler.
GT	Gas turbine.
HESS	Hydrogen energy storage system.
HSS	Heating storage system.
HV	Hydrogen vehicle.
IES	Integrated energy systems.
LCA	Life cycle assessment.
PDN	Power distribution network.

The associate editor coordinating the review of this manuscript and approving it for publication was Amin Mahmoudi.

PEM	Proton exchange membrane.
PV	Photovoltaic.
SOC	State of charge.
WHB	Waste heat boiler.
WT	Wind turbine.

INDICES

i, j	Indices of PDN nodes.
n	Indices of equipment.
t	Indices of time.
k	The type of raw material for equipment.
m, b	Indices of pipeline nodes.

PARAMETERS

c_n	The unit capacity investment cost.
β_n	The depreciation factor.
λ_p, λ_v	The economic coefficient of active network losses and voltage deviation.
R_i	The resistance value of the branch.
V_{jN}	The nominal voltage of the node.
$A_{PV}^{\max}$	Maximum possible area of the PV.
$P_{WT}^{\max}$	Maximum possible capacity of the WT.
$N_{FC}^{\max}$	Maximum possible capacity of the FC.
$N_{HESS}^{\max}$	Maximum possible capacity of the HESS.
v_{ci}, v_{ra}, v_{out}	The cut-in, rated, and cut-out wind speeds.
η_{PV}	The conversion efficiency of the PV.
η_{PEM}	The conversion efficiency of the PEM electrolyzer.
$P_{PEM}^{\max}$	Maximum electrical power consumption of the PEM electrolyzer.
$Q_{PEM}^{\max}$	Maximum hydrogen production in PEM electrolyzer.
$\eta_H^{chr}, \eta_H^{dis}$	The charging and discharging conversion efficiency of the HESS.
$\lambda_{hess}^{\min}, \lambda_{hess}^{\max}$	Minimum and maximum coefficients of HESS storage capacity.
λ_{FC}	The electrical conversion efficiency of the FC.
$E_j^{t,bef}$	Node electrical load.
$E_{load}^{t,bef}$	Regional electrical load.
$H_{load}^{t,bef}$	Regional heat load.
s_{gas}^t, s_{grid}^t	Natural gas and grid power price.
s_{gt}, s_{gb}, s_{whb}	The operating cost of the GT, GB, and WHB, respectively.
$s_{ae}, s_{es}, s_{hs}, s_{fc}, s_{hess}$	The operating cost of the AE, ESS, HSS, FC, and HESS, respectively.
s_{CO_2}	The economic coefficient of carbon emissions.
s_{pv}, s_{wt}	The operating cost of the PV and WT.
$s_{fc}, s_{pem}, s_{hess}$	The operating cost of the FC, PEM electrolyzer, and HESS.
L_{NVNG}	The heating value of natural gas.
η_{GT}	The conversion efficiency of the GT.
$P_{GT}^{\min}, P_{GT}^{\max}$	Minimum and maximum power generation of the GT.
λ_{GT}	The electrical-to-thermal ratio of the GT.
λ_{re}	The recovery efficiency.
$H_{WHB}^{\min}, H_{WHB}^{\max}$	Minimum and maximum thermal energy generation of the WHB.
$\eta_{ES}^{chr}, \eta_{ES}^{dis}$	The charging and discharging efficiencies of the ESS.
$E_{ES}^{\min}, E_{ES}^{\max}$	Minimum and maximum stored energy of the ESS.
$P_{ES}^{\max}$	Maximum charging and discharging power of the ESS.
$E_{HS}^{\min}, E_{HS}^{\max}$	Minimum and maximum stored energy of the HSS.
$\eta_{HS}^{chr}, \eta_{HS}^{dis}$	The charging and discharging efficiencies of the HSS.
$H_{HS}^{\max}$	Maximum charging and discharging thermal power of the HSS.
$\eta_{AE,e}, \eta_{AE,h}$	The hydrogen and heat production efficiencies of the AE.
q_{H_2}	The conversion ratio of hydrogen.
$P_{AE}^{\max}$	Maximum power consumption of the AE.
$\eta_{FC,e}, \eta_{FC,h}$	The electrical and thermal efficiencies of the FC.
$Q_{HESS}^{\max}$	Maximum hydrogen charging and discharging of the HESS.
λ_{ms}	The hydrogen recovery rate.
$Q_{g,mn}^{\max}$	Maximum transmission flow rate in a pipeline.
e_{grid}, e_{GT}, e_{GB}	The carbon emissions per unit of electricity supplied by the upper grid, GT, and GB, respectively.
$M_{n,k}$	The type of raw material for equipment.
$EF_{n,k}$	The carbon emissions generated from the production of the kth type of raw material.
E_{em}	The energy consumed during production.
EF_n^e	The carbon emissions associated with this electricity.
EF_n^{re}	The unit electricity carbon emissions for the WT and PV.
$L_k^{Cap,t}, L_k^{Cap,\max}$	The actual traffic capacity and road capacity of road segment.
v^{rl}	Maximum driving speed for the different road classifications.

λ_{hev}	The energy consumption coefficient.
e^t_{ev}, e^t_{hev}	The driving energy consumption of the EV and HV.

VARIABLES

N_n	The investment capacity.
P_i	The active power of the node.
Q_i	The reactive power of the node.
V_j	Voltage of node.
A_{PV}	Area of the PV.
P^{ra}_{WT}	Capacity of the WT.
N_{FC}	Capacity of the FC.
N_{HESS}	Capacity of the HESS.
$P^{pre}_{WT,t}$, $P^{pre}_{PV,t}$	Predictive power generation of WT and PV.
P^t_{WT}, $P^t_{WT,cur}$	The utilized and curtailed power of the WT.
P^t_{PV}, $P^t_{PV,cur}$	The utilized and curtailed power of the PV.
v_t, $G_{PV,t}$	Wind speed and solar irradiance.
P^t_{PEM}	The electrical energy required by the PEM electrolyzer.
Q^t_{PEM}	The hydrogen produced by PEM electrolyzer.
$d^{t,des}_{hess,chr}$, $d^{t,des}_{hess,dis}$	The charging and discharging binary state coefficients of the HESS in the EHIES.
$d^{t,ies}_{hess,chr}$, $d^{t,ies}_{hess,dis}$	The charging and discharging binary state coefficients of the HESS in the IES.
$E^t_{H,des}$	The amount of hydrogen stored in the HESS in the EHIES.
$E^t_{H,ies}$	The amount of hydrogen stored in the HESS in the IES.
$Q^t_{FC,des}$	The hydrogen consumption of the FC in the EHIES.
$P^t_{FC,des}$	The power generation of the FC in EHIES.
P_{ij}, Q_{ij}	Active power flow and reactive power flow of line.
p_j, q_j	Active power and reactive power injected of node.
I_{ij}	Current of branch.
$P^t_{des,c}$	The low-carbon electricity provided by EHIES to IES..
V^t_{GT}, V^t_{GB}	The natural gas volume for the GT and GB, respectively.
P^t_{buy}	Purchased electricity from the upper grid.
P^t_{GT}	The power generation of the GT.
H^t_{GB}, H^t_{WHB}, H^t_{AE}	The thermal generation of the GB, WHB, and AE, respectively.
$P^t_{FC,ies}$	The power generation of the FC in IES.
$P^t_{ES,chr}$, $P^t_{ES,dis}$	The charging and discharging power of the ESS.
$d^t_{es,chr}$, $d^t_{es,dis}$	The charging and discharging binary state coefficients of the ESS.
$d^t_{hs,chr}$, $d^t_{hs,dis}$	The charging and discharging binary state coefficients of the HSS.
$H^t_{HS,chr}$, $H^t_{HS,dis}$	The heat absorption and release of the HSS.
$Q^{t,ies}_{HESS,chr}$, $Q^{t,ies}_{HESS,dis}$	The hydrogen charging and discharging of the HESS in IES.
$P^t_{ies,c}$	The low-carbon electricity obtained by IES from EHIES..
ρ^t_{pdn}	The carbon emission density of the PDN.
LC_n	The lifecycle carbon emissions of equipment.
$H^t_{GT,WHB}$	Thermal energy supplied by GT to WHB.
H^t_{GT}	The thermal generation of the GT.
E^t_{ES}, E^t_{HS}	The amount of energy stored in the ESS and HSS.
P^t_{AE}	The power consumption of the AE.
Q^t_{AE}	Hydrogen production from AE.
$Q^t_{AE,FC}$, $Q^t_{AE,FCS}$	The quantity of hydrogen supplied from the AE to the FC and FCS.
$Q^t_{FC,ies}$	The hydrogen consumption of the FC in the IES.
$H^t_{FC,ies}$	The thermal generation of the FC in the IES.
L^n_{hev}	The hydrogen charging demand for regional HVs.
L^n_{ev}	The charging demand for regional EVs.
Q^t_g, $Q^t_{g,gas}$, $Q^t_{g,H}$	The amount of mixed gas, natural gas, and hydrogen in the natural gas pipeline, respectively.
Q^t_{ms}	The amount of separated hydrogen.
D^t_{grid}, D^t_{GB}, D^t_{ES}	The carbon emissions of the upper grid, GB, and ESS.
$D^t_{GT,e}$, $D^t_{GT,h}$	The carbon emissions from the GT for electricity generation and heat production, respectively.
EF^{IES}_{ccer}	The carbon emission coefficient per unit of electricity used by an IES.
$V^t_{L_k}$	The driving speed of vehicles on road segment.

I. INTRODUCTION

A. MOTIVATIONS

As fossil fuel consumption and environmental degradation continue, the proportion of renewable energy sources in the global energy mix is consistently rising. Projections indicate that renewable energy will represent a substantial segment of the global energy supply, estimated to range between 23%

and 42% by 2040 [1]. However, as hydrogen production and storage technologies advance, the integration of energy sources like wind power, solar energy, and hydrogen becomes possible. The addition of this new energy system poses new challenges to IES [2]. Hydrogen energy has the potential to be integrated into IES alongside energy storage systems (ESS) and electric vehicles (EVs) as a storage solution. Such integration has the potential to significantly enhance the reliability, cost-effectiveness, and reduce carbon emissions of the IES [3], [4]. Moreover, existing carbon emission studies primarily focus on the carbon emissions generated by equipment such as gas turbines (GT) and gas boilers (GB), while overlooking the carbon emissions produced by renewable energy generation and hydrogen energy storage systems (HESS) throughout their entire lifecycle [5]. LCA serves as a method for evaluating the carbon emissions generated throughout the entire lifecycle of equipment, from manufacturing to disposal [6]. It can effectively evaluate the carbon emissions produced by renewable energy generation and hydrogen system throughout their entire lifecycle. Therefore, the coordinated planning of an EHIES that considers lifecycle carbon emissions is of significant practical importance for enhancing the economic efficiency and reducing the carbon emissions of IES.

B. LITERATURE REVIEW

The combination of renewable energy and hydrogen system is beneficial for achieving low-carbon and clean IES. In [7], a microgrid energy system that integrates photovoltaics (PV), hydrogen system, EVs, and Z-source converters was presented. This system was optimized through an Energy management strategy (EMS) using biogeography-based optimization algorithms. Reference [8] focused on the development of a sophisticated distributed PV system through the analysis of meteorological data. The system was integrated into a distributed hydrogen thermal storage system (DHTSS) to optimize economic costs and minimize the curtailment of excess solar power. In [9], hydrogen production was integrated with the electricity and hydrogen markets. The optimization of economic costs and profits for system operators was achieved through the application of Markov decision process theory. The integration of hydrogen and water into energy systems aimed to enhance the overall economic efficiency. In [10], an optimal energy storage scheduling model for an IES that includes hydrogen and water was presented. The primary objective was to optimize and enhance the economic aspects of the system. Reference [11] introduced a dynamic balance feedback control strategy for an electric-thermal coupling production scheme. This strategy focused on optimizing the capacity allocation of the devices within hydrogen-containing regional IES. The optimization was performed using a multi-objective chaotic particle swarm algorithm that incorporated greedy and elite preservation strategies. In [12], a bi-level optimization model for a regional IES was constructed. This model aimed to find balanced solutions between the equipment quantities and capacities.

In the meantime, scholars have actively expanded the field of planning for distributed energy system (DES). In [13], a wind-hydrogen energy system (W-HES) was established, utilizing surplus wind power for hydrogen production and storing this hydrogen in HESS to enhance energy efficiency. In [2], a bi-level planning model for a hydrogen IES was proposed, considering multi-stage investment and carbon trading mechanisms. This model proved effective in reducing the operational costs and carbon emissions of this system. In [14], a distributed energy device comprising fuel cells (FC), electrolyzers, and HESS was constructed and integrated into the PDN. In [15], a method was proposed for hydrogen production using solar thermochemical processes and for electricity generation with FCs, achieving a cascaded utilization of FCs and solar energy. Reference [16] introduced a model for integrating hydrogen into renewable energy systems. This model involved the production of hydrogen from surplus or curtailed renewable energy when wind turbine (WT), biogas plants, and PV satisfied the demands of residential and commercial loads. The coupling of PDN with the natural gas network [17], and the blending of natural gas with hydrogen, facilitates the low-carbon operation of the system [18]. Therefore, hydrogen energy equipment that serves as a carrier of low-carbon energy, can be readily integrated into DES. From the above studies, it can be seen that current research on DES planning only involves the coupling of some renewable energy sources with hydrogen, and there is no proposed modeling and planning method for integrating wind, solar, and hydrogen systems together (see Table 1).

An energy system incorporating hydrogen plays a crucial role in achieving low-carbon energy systems [19], [20]. While some studies have considered the economic aspect of IES and incorporated the reduction of carbon emissions as an objective function (as shown in Table 1), these studies primarily focus on carbon trading mechanisms. In [21], small-scale nuclear power units and carbon trading were introduced into an IES. Reference [22] put forth a gradual carbon trading approach for computing carbon trading within the combined heat and power (CHP) and hydrogen system. In [23], it was suggested to combine demand response (DR) with carbon trading to promote user engagement in DR within IES, ultimately lowering costs for users and load aggregators. Nonetheless, the prices and transactions in these trading mechanisms frequently overlook interactions among parties. Consequently, in [24], a cooperative game-based profit allocation mechanism was introduced to enhance the revenue of IES with HESS and minimize carbon emissions. In [25], a carbon trading mechanism for Chinese Certified Emission Reductions (CCER) based on the Vickrey auction was introduced. This mechanism employs a sealed-bid auction format where the highest bidder obtains carbon emission allowances. Subsequently, the process continues with the next round of bidding at the second-highest price. This approach is applied to integrated heat-power-hydrogen energy systems with the

TABLE 1. Comparison with several related reference.

Refs	Coupling Resources	Energy storage type	Energy storage Utilization form	Planning and optimization objectives
[7]	Solar and hydrogen energy	ESS, HESS	Electricity, hydrogen	Maximize energy efficiency
[8]	Solar and hydrogen energy	HSS, HESS	Electricity, heat	Highest power supply reliability
[9]	Wind and hydrogen energy	HESS	Electricity, hydrogen	Highest economic reliability
[10]	Hydrogen energy	HESS, water storage	Electricity, heat	Minimize energy cost and carbon emission
[11]	Hydrogen energy	HESS	Electricity, heat	Minimize economy and carbon emission, highest energy efficiency
[12]	Wind and solar energy	HESS	Electricity, heat	Maximize energy efficiency
[13]	Wind and hydrogen energy	HESS	Electricity, hydrogen	Minimize economic cost
[14]	Hydrogen energy	HESS	Electricity	Minimize power losses and maximize energy efficiency
[15]	Solar and hydrogen energy	-	Electricity, heat	Highest energy efficiency
[16]	Hydrogen energy	HESS	Electricity	Highest economy, low carbon and energy efficiency
[18]	Nature gas and hydrogen energy	-	Electricity, heat, hydrogen	Minimize operating cost and maximize transaction payment
[21]	Nuclear	ESS, HSS	Electricity, heat	Maximize system economic and environmental benefit
[22]	Wind and hydrogen energy	ESS, HESS	Electricity, heat	Minimize carbon emission and operating cost
[24]	Hydrogen energy	HESS	Electricity, heat	Minimize carbon emission and operating cost
[25]	Hydrogen energy	ESS, HESS	Electricity, heat	Highest economy, low carbon
This paper	Solar, Wind, and hydrogen energy	ESS, HSS, HESS	Electricity, heat, hydrogen	Minimize power losses cost, voltage deviation costs, operating cost and lifecycle carbon emissions

aim of reducing the overall carbon emissions of the system. However, due to the supply-demand disparities among different IESs, directly implementing a carbon trading mechanism in the EHIES planning to reduce the carbon emissions of the IES system is not feasible. Therefore, it is of utmost importance to consider the impact on the total carbon emissions of IES and find a suitable method to plan EHIES.

C. CONTRIBUTION AND ORGANIZATION OF THE PAPER

In summary, existing DES should include and take into account hydrogen energy equipment to improve system stability and lower carbon emissions. However, current research fails to account for the influence of equipment lifecycle carbon emissions on the total carbon footprint in the planning phase. To address these concerns, this study delves into EHIES planning by considering lifecycle carbon emissions linked to renewable energy sources. Moreover, it examines the cooperative operation of the IES along with the EHIES. The primary contributions of this study are as follows:

(1) The EHIES is developed by incorporating PV, WT, proton exchange membrane (PEM) electrolyzer, HESS, and FC. Furthermore, the planning considers the demand from both EVs and hydrogen vehicles (HV) within the specified area.

(2) Employing carbon flow to allocate decarbonization responsibilities among users, the study assesses the carbon emissions generated by the electricity supply within the IES. Additionally, the LCA method is utilized to analyze the carbon emissions of new energy and hydrogen equipment, allowing for a more accurate calculation of equipment lifecycle carbon emissions within the EHIES.

(3) In the first stage, the planning location and equipment capacity of EHIES are determined with the objective of minimizing investment costs, lifecycle carbon emissions, and improving the operational stability of PDN. In the second stage, EHIES and IES coordinate operations to reduce carbon emissions and operating costs.

The subsequent sections of this paper are organized as follows: Section II introduces the planning and operational models. Section III outlines the methodology used to solve the models. Section IV presents the numerical results of case studies. Finally, Section V offers concluding remarks.

II. FORMULATIONS

In this section, we first present the EHIES planning model. Next, we introduce a coordinated operation model that incorporates subsidies for carbon emissions. Finally, this model is applied to a two-stage planning model.

A. EHIES PLANNING MODEL

The EHIES system comprises the PV, WT, PEM electrolyzer, HESS, and FC. PEM electrolyzer exhibits high electrolysis efficiency, rapid start-stop capabilities, and the production of high-purity hydrogen gas. This makes it ideal for converting the surplus energy generated by PV and WT into hydrogen gas, which is subsequently stored in the HESS. The FC utilizes hydrogen gas from the HESS to provide electricity, meeting peak system power demands and enhancing system stability. The architecture of the EHIES is shown in Fig. 1.

In the first stage, the aim is to determine the optimal location and capacity of the EHIES connections to the PDN. Additionally, based on the equipment capacity obtained in this stage, the lifecycle carbon emissions of EHIES will be calculated, and the calculation method will be detailed in Section B of Chapter III. The objective of this stage is to minimize investment costs, active network loss costs, lifecycle carbon emissions costs and voltage deviation costs. The formula for this calculation is as follows:

$$F_1 = \min(C_{inv} + C_p + C_v + C_{ccer}) \tag{1}$$

$$\begin{cases} C_{inv} = \sum_n c_n \cdot \beta_n \cdot N_n \\ C_p = \lambda_p \sum^{D} \dfrac{P_i^2 + Q_i^2}{V_j^2} R_i \\ C_v = \lambda_v \sum^{D} \dfrac{\left|V_j - V_{jN}\right|}{V_{jN}} \\ C_{ccer} = s_{CO_2} \sum_n LC_n \end{cases}$$

$$n \in \{WT, PV, PEM, HESS, FC\} \tag{2}$$

where F_1 is the objective function of the first stage. C_{inv}, C_p, C_{ccer}, and C_v represent the investment costs, active network loss costs, lifecycle carbon emissions costs, and voltage deviation costs, respectively. c_n denotes the unit capacity investment cost. β_n denotes the depreciation coefficient. N_n is equipment investment capacity. λ_p is the economic coefficient of active network losses. λ_v is the economic coefficient of the voltage deviation. P_i is the active power of the node. Q_i is the reactive power of the node. V_j is the node voltage. R_i is the resistance value of the branch. V_{jN} is the nominal voltage of the node. s_{CO_2} is the economic coefficient of carbon emissions. LC_n is the lifecycle carbon emissions of equipment n.

The model encompasses investment, operational, and energy balance constraints. These constraints are detailed as follows.

1) INVESTMENT CONSTRAINTS

$$0 \le A_{PV} \le A_{PV}^{\max} \tag{3}$$
$$0 \le P_{WT}^{ra} \le P_{WT}^{\max} \tag{4}$$
$$0 \le N_{FC} \le N_{FC}^{\max} \tag{5}$$
$$0 \le N_{HESS} \le N_{HESS}^{\max} \tag{6}$$

where A_{PV} denotes the planned PV area. $A_{PV}^{\max}$ represents the maximum PV area. P_{WT}^{ra} is the planned rated power of the WT. $P_{WT}^{\max}$ is the maximum rated power of a WT. N_{FC} denotes the planned FC capacity. $N_{FC}^{\max}$ is the maximum capacity of the FC. $N_{HESS}^{\max}$ is the upper capacity limit of the HESS. N_{HESS} is the planned capacity of the HESS.

2) OPERATIONAL CONSTRAINTS

The operational constraints of the EHIES include the WT, PV, PEM electrolyzer, FC, HESS, and PDN.

The constraints for WT and PV are as follows.

$$P_{WT,t}^{pre} = \begin{cases} 0 & v_t < v_{ci} \\ \dfrac{P_{WT}^{ra}(v_t - v_{ci})}{(v_{ra} - v_{ci})} & v_{ci} \le v_t < v_{ra} \\ P_{WT}^{ra} & v_{ra} \le v_t < v_{out} \\ 0 & v_t \ge v_{out} \end{cases} \tag{7}$$

$$P_{WT,t}^{pre} = P_{WT}^{t} + P_{WT,cur}^{t} \tag{8}$$
$$P_{PV,t}^{pre} = \eta_{PV} A_{PV} G_{PV,t} \tag{9}$$
$$P_{PV,t}^{pre} = P_{PV}^{t} + P_{PV,cur}^{t} \tag{10}$$

where $P_{WT,t}^{pre}$ is the output power of the WT. v_{ci}, v_{ra} and v_{out} represent the cut-in, rated, and cut-out wind speeds, respectively. $P_{PV,t}^{pre}$ represents the output power of the PV system. η_{PV} is the conversion efficiency. $G_{PV,t}$ is solar irradiance.

The constraints of PEM electrolyzer are as follows.

$$Q_{PEM}^{t} = \eta_{PEM} P_{PEM}^{t} \tag{11}$$
$$P_{PEM}^{t} = P_{PV,cur}^{t} + P_{WT,cur}^{t} \tag{12}$$
$$0 \le Q_{PEM}^{t} \le Q_{PEM}^{\max} \tag{13}$$
$$0 \le P_{PEM}^{t} \le P_{PEM}^{\max} d_{hess,chr}^{t} \tag{14}$$

where Q_{PEM}^{t} is the hydrogen produced by PEM electrolyzer. P_{PEM}^{t} is the electrical energy required by the PEM electrolyzer. η_{PEM} is the conversion efficiency. $P_{PV,cur}^{t}$ and $P_{WT,cur}^{t}$ are the curtailed solar and wind power, respectively. $Q_{PEM}^{\max}$ is the maximum hydrogen production in PEM electrolyzer. $P_{PEM}^{\max}$ is the maximum electrical power consumption of the PEM electrolyzer.

The constraints of HESS are as follows.

$$E_{H,des}^{t} = \begin{cases} E_{H,des}^{t-1} + \eta_H^{chr} Q_{PEM}^{t} & d_{hess,chr}^{t,des} = 1 \\ E_{H,des}^{t-1} + Q_{FC,des}^{t} \Big/ \eta_H^{dis} & d_{hess,dis}^{t,des} = 1 \end{cases} \tag{15}$$

$$E_{H,des}^{1} = E_{H,des}^{T} \tag{16}$$
$$\lambda_{hess}^{\min} N_{HESS} \le E_{H,des}^{t} \le \lambda_{hess}^{\max} N_{HESS} \tag{17}$$

where $E_{H,des}^{t}$ is the amount of hydrogen stored in the HESS. $\lambda_{hess}^{\min}$ and $\lambda_{hess}^{\max}$ are the minimum and maximum coefficients of HESS storage capacity, respectively. $d_{hess,chr}^{t,des}$ and $d_{hess,dis}^{t,des}$ are charging and discharging binary state coefficients of HESS (with 0-1 variables), respectively. $Q_{FC,des}^{t}$ is the FC hydrogen consumption. η_H^{chr} and η_H^{dis} represent the hydrogen charging and discharging efficiency of the HESS, respectively.

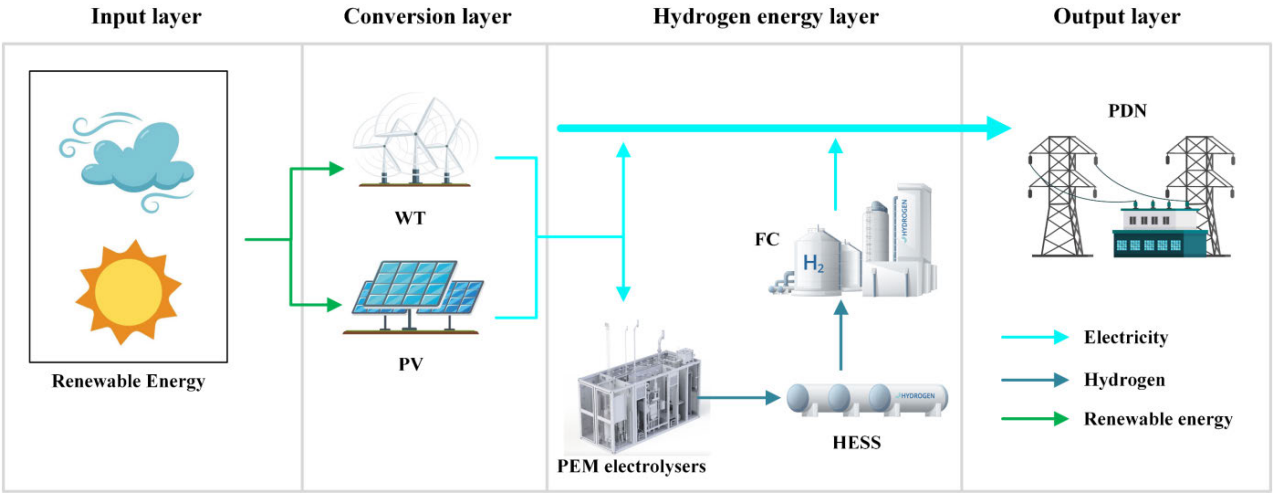

FIGURE 1. The architecture of the EHIES.

The constraints of FC are as follows.

$$P^t_{FC,des} = Q^t_{FC,des} \cdot N_{FC} \frac{\lambda_{FC}}{N^{\max}_{FC}} \tag{18}$$

$$0 \le Q^t_{FC,des} \le Q^{\max}_{PEM} d^t_{hess,dis} \tag{19}$$

where $P^t_{FC,des}$ denotes the power generation of the FC. λ_{FC} is the electrical conversion efficiency at the maximum capacity.

The branch power flow constraints of the PDN model based on second-order cone relaxation optimization are as follows.

$$\begin{cases} p_j = \sum_{k\in\delta(j)} P_{jk} - \sum_{i\in\pi(j)} (P_{ij} - \tilde{I}_{ij} r_{ij}) + g_j \tilde{V}_j, \forall j \in B \\ q_j = \sum_{k\in\delta(j)} Q_{jk} - \sum_{i\in\pi(j)} (Q_{ij} - \tilde{I}_{ij} r_{ij}) + b_j \tilde{V}_j, \forall j \in B \end{cases} \tag{20}$$

$$\tilde{V}_j = \tilde{V}_i - 2(P_{ij} r_{ij} + Q_{ij} x_{ij}) + \tilde{I}_{ij}(r^2_{ij} + x^2_{ij}), \forall ij \in E \tag{21}$$

$$\left\| \begin{matrix} 2P_{ij} \\ 2Q_{ij} \\ \tilde{I}_{ij} - \tilde{V}_j \end{matrix} \right\|_2 \le \tilde{I}_{ij} + \tilde{V}_j, \forall ij \in E \tag{22}$$

$$I^2_{ij} \le \tilde{I}_{ij} \le \bar{I}^2_{ij}, \forall ij \in E \tag{23}$$

$$V^2_j \le \tilde{V}_j \le \bar{V}^2_j, \forall j \in B^+ \tag{24}$$

where p and q represent the node-injected active and reactive powers, respectively. P and Q represent the active and reactive powers of the branch currents, respectively. V is the node voltage. I is the branch current, where $\tilde{I}_{ij} = I^2_{ij}$, $\tilde{V}_j = V^2_j$.

3) ENERGY BALANCE CONSTRAINT

The electrical balance constraint of EHIES is as follows.

$$E^{t,bef}_j + P^t_{PEM} + P^t_{des,c} = P^t_{PV} + P^t_{WT} + P^t_{FC,des} \tag{25}$$

where: $P^t_{des,c}$ is the low-carbon electricity provided by EHIES to IES.

B. COODINATED OPERATION MODEL

The IES purchases natural gas from gas companies and electricity from upper grid to bridge the supply-demand gaps. There are four types of energy exchange between components: natural gas, electricity, thermal energy, and hydrogen energy. The PDN transmits electrical energy to consumers. The AE serves as the primary hydrogen production equipment in the IES. The hydrogen produced is sent to the HESS and can be converted into electrical energy by the FC as needed. Natural gas is converted into thermal and electrical energies. The electrical energy generated by the GT is distributed through power lines to the region, while the thermal energy produced is conveyed to a Waste Heat Boiler (WHB) connected to the primary heating network. The GB uses natural gas to generate thermal energy for regional heating. HESS, ESS, and heating storage system (HSS) store surplus hydrogen, electricity, and thermal energy for use during peak energy demand. The architecture of the IES is shown in Fig. 2.

To reduce IES carbon emissions, promote clean energy power generation, and decrease electricity from conventional power sources. Providing economic subsidies to EHIES based on the difference in carbon emissions between IES and EHIES incentivizes EHIES to supply more low-carbon electricity to IES. For the IES, the objective function aims to minimize operating costs, and carbon emission subsidies, as follows:

$$F_2 = \min\left(C^{IES}_{om} + C^{IES}_{ces}\right) \tag{26}$$

$$\begin{cases} C^{IES}_{om} = \sum_t \left[\begin{matrix} s^t_{gas}\left(V^t_{GT} + V^t_{GB}\right) + s^t_{grid} P^t_{buy} + s_{gt} P^t_{GT} + \\ s_{gb} H^t_{GB} + s_{whb} H^t_{WHB} + s_{fc} P^t_{FC,ies} + \\ s_{ae} H^t_{AE} + s_{es}(P^t_{ES,chr} + P^t_{ES,dis}) + \\ s_{hs}(H^t_{HS,chr} + H^t_{HS,dis}) + \\ s_{hess}(Q^{t,ies}_{HESS,chr} + Q^{t,ies}_{HESS,dis}) \end{matrix} \right] \\ C^{IES}_{ces} = s_{CO_2}\left(\sum_{t=1}^{24} \rho^t_{pdn} \cdot P^t_{ies,c} - \sum_n LC_n \right) \end{cases} \tag{27}$$

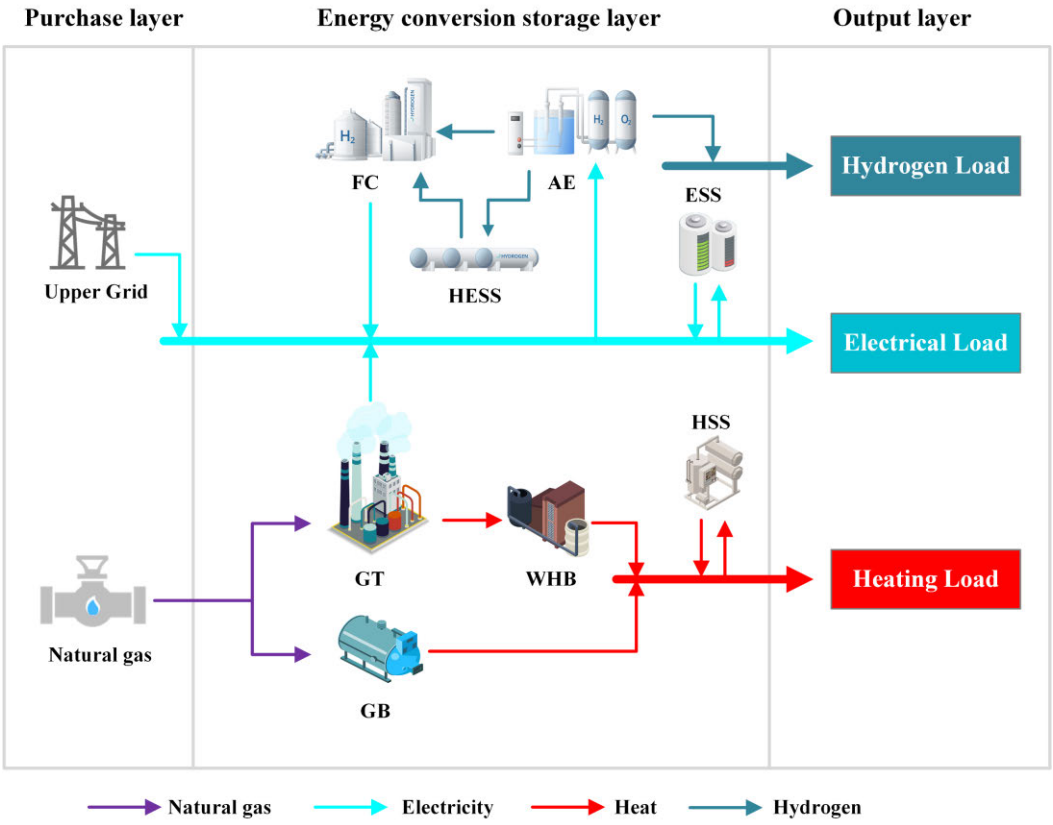

FIGURE 2. The architecture of the IES.

where F_2 denotes the total operating cost of the IES. C_{om}^{IES} and C_{ces}^{IES} represent operating costs and carbon emissions subsidies, respectively. s_{gas}^t, s_{grid}^t, s_{gt}, s_{gb}, s_{whb}, s_{ae}, s_{es}, s_{hs}, s_{fc},and s_{hess} represent natural gas price, electricity price, GT operating cost, GB operating cost, WHB operating cost, AE operating cost, ES operating cost, HS operating cost, FC operating cost, and HESS operating cost, respectively. $P_{ies,c}^t$ represents the low-carbon electricity obtained by IES from EHIES. ρ_{pdn}^t is the carbon emission density of the PDN.

The EHIES acts as a system that couples renewable energy with hydrogen. It generates low-carbon electricity to supply the IES while meeting local electricity demand. This effectively reduces carbon emissions from the IES. To incentivize the EHIES to provide more low-carbon electricity, the IES will offer a carbon emission subsidy to the EHIES system [26]. The objective function for the EHIES is to minimize operating costs while maximizing earned carbon emission subsidies, as follows:

$$F_3 = \min C_{om}^{DES} + \max C_{ces}^{DES} \tag{28}$$

$$\begin{cases} C_{om}^{DES} = \sum_t \left[\begin{array}{l} s_{pv} P_{PV}^t + s_{wt} P_{WT}^t + s_{fc} P_{FC,des}^t \\ + s_{pem} P_{PEM}^t + s_{hess} \left(Q_{FC,des}^t + Q_{PEM}^t \right) \end{array} \right] \\ C_{ces}^{DES} = s_{CO_2} \left(\sum_{t=1}^{24} \rho_{pdn}^t \cdot P_{des,c}^t - \sum_n LC_n \right) \end{cases} \tag{29}$$

where F_3 denotes the total operating cost of the EHIES. C_{om}^{DES} and C_{ces}^{DES} represent the operating costs and earned carbon emissions subsidies, respectively. s_{pv}, s_{wt},and s_{pem} represent the operating costs of the PV, WT, and PEM electrolyzer, respectively.

The model encompasses the operation, energy balance, and shared natural-gas pipeline constraints of the IES. These constraints are detailed as follows.

1) OPERATIONAL CONSTRAINTS

The constraints of GT are as follows.

$$P_{GT}^t = V_{GT}^t L_{NVNG} \eta_{GT} \tag{30}$$

$$H_{GT}^t = P_{GT}^t / \lambda_{GT} \tag{31}$$

$$P_{GT}^{\min} \le P_{GT}^t \le P_{GT}^{\max} \tag{32}$$

where the GT output P_{GT}^t depends on the gas volume V_{GT}^t. L_{NVNG} is the heating value of natural gas. η_{GT} is the conversion efficiency. H_{GT}^t represents the thermal energy generated. λ_{GT} is the electrical-to-thermal ratio of the GT. $P_{GT}^{\max}$ and $P_{GT}^{\min}$ are the upper and lower limits of the GT output, respectively.

The constraints of WHB are as follows.

$$H_{WHB}^t = \lambda_{re} H_{GT,WHB}^t \tag{33}$$

$$H_{WHB}^{\min} \le H_{WHB}^t \le H_{WHB}^{\max} \tag{34}$$

$$0 \le H_{GT,WHB}^t \le H_{GT}^t \tag{35}$$

where H^t_{WHB} denotes the thermal energy generated by the WHB. $H^t_{GT,WHB}$ represents the thermal energy provided by the GT to the WHB. λ_{re} is the recovery efficiency. $H^{\max}_{WHB}$ and $H^{\min}_{WHB}$ represent the upper and lower limits of thermal energy produced by the WHB, respectively.

The constraints of ESS are as follows.

$$E^t_{ES} = \begin{cases} E^{t-1}_{ES} + \eta^{chr}_{ES} P^t_{ES,chr} & d^t_{es,chr} = 1 \\ E^{t-1}_{ES} + P^t_{ES,dis} \Big/ \eta^{dis}_{ES} & d^t_{es,dis} = 1 \end{cases} \tag{36}$$

$$E^1_{ES} = E^T_{ES} \tag{37}$$

$$E^{\min}_{ES} \le E^t_{ES} \le E^{\max}_{ES} \tag{38}$$

$$\begin{cases} 0 \le P^t_{ES,chr} \le P^{\max}_{ES} d^t_{es,chr} \\ 0 \le P^t_{ES,dis} \le P^{\max}_{ES} d^t_{es,dis} \end{cases} \tag{39}$$

$$d^t_{es,chr} + d^t_{es,dis} \le 1 \tag{40}$$

where E^t_{ES} denotes the amount of energy stored in the ESS. $P^t_{ES,chr}$ and $P^t_{ES,dis}$ represent the charging and discharging power of the ESS, respectively. η^{chr}_{ES} and η^{dis}_{ES} represent the charging and discharging efficiencies of the ESS, respectively. $d^t_{es,chr}$ and $d^t_{es,dis}$ represent the charging and discharging binary state coefficients of ESS (with 0-1 variables), respectively. $E^{\min}_{ES}$ and $E^{\max}_{ES}$ represent the upper and lower limits of the stored energy within the ESS, respectively. $P^{\max}_{ES}$ represents the maximum charging and discharging powers of the ESS.

The constraints of HSS are as follows.

$$E^t_{HS} = \begin{cases} E^{t-1}_{HS} + \eta^{chr}_{HS} H^t_{HS,chr} & d^t_{hs,chr} = 1 \\ E^{t-1}_{HS} + H^t_{HS,dis} \Big/ \eta^{dis}_{HS} & d^t_{hs,dis} = 1 \end{cases} \tag{41}$$

$$E^1_{HS} = E^T_{HS} \tag{42}$$

$$E^{\min}_{HS} \le E^t_{HS} \le E^{\max}_{HS} \tag{43}$$

$$\begin{cases} 0 \le H^t_{HS,chr} \le H^{\max}_{HS} d^t_{hs,chr} \\ 0 \le H^t_{HS,dis} \le H^{\max}_{HS} d^t_{hs,dis} \end{cases} \tag{44}$$

$$d^t_{hs,chr} + d^t_{hs,dis} \le 1 \tag{45}$$

where E^t_{HS} is the amount of energy stored in the HSS. $H^t_{HS,chr}$ and $H^t_{HS,dis}$ are the heat absorption and release of the HSS. η^{chr}_{HS} and η^{dis}_{HS} represent the heat absorption and release efficiencies of the HSS, respectively. $d^t_{hs,chr}$ and $d^t_{hs,dis}$ are the heat absorption and release binary state coefficients of the HSS (with 0-1 variables), respectively. $E^{\min}_{HS}$ and $E^{\max}_{HS}$ are the upper and lower limits of the stored energy within the HSS, respectively. $H^{\max}_{HS}$ represents the maximum heat absorption and release of the HSS.

The constraints of AE are as follows.

$$Q^t_{AE} = \eta_{AE,e} \frac{P^t_{AE}}{q_{H_2}} \tag{46}$$

$$H^t_{AE} = \eta_{AE,h} \left(1 - \eta_{AE,e}\right) P^t_{AE} \tag{47}$$

$$Q^t_{AE} = Q^t_{AE,FC} + Q^t_{AE,FCS} + Q^{t,ies}_{HESS,chr} \tag{48}$$

$$0 \le P^t_{AE} \le P^{\max}_{AE} \tag{49}$$

where Q^t_{AE} is the amount of hydrogen produced by the AE. P^t_{AE} represents the power consumption of the AE. H^t_{AE} is the thermal generation of the AE. q_{H_2} is the conversion ratio of hydrogen. $\eta_{AE,e}$ and $\eta_{AE,h}$ represent the hydrogen and heat production efficiencies of the AE, respectively. $Q^t_{AE,FC}$ represents the amount of hydrogen supplied by the AE to the FC. $Q^t_{AE,FCS}$ represents the amount of hydrogen supplied by the AE to the fast-charging stations (FCS). $Q^{t,ies}_{HESS,chr}$ represents the amount of hydrogen supplied by the AE to the HESS. $P^{\max}_{AE}$ is the maximum power consumption of the AE.

The constraints of FC are as follows.

$$P^t_{FC,ies} = Q^t_{FC,ies} \cdot \eta_{FC,e} \cdot q_{H_2} \tag{50}$$

$$H^t_{FC,ies} = \eta_{FC,h} \left(1 - \eta_{FC,e}\right) P^t_{FC,ies} \tag{51}$$

$$Q^t_{FC,ies} = Q^t_{AE,FC} + Q^{t,ies}_{HESS,dis} \tag{52}$$

where $P^t_{FC,ies}$ denotes the power generation of the FC in the IES. $H^t_{FC,ies}$ is the thermal generation of the FC in the IES. $\eta_{FC,e}$ and $\eta_{FC,h}$ represent the electrical and thermal efficiencies of the FC, respectively. $Q^t_{FC,ies}$ is the hydrogen consumption of the FC.

The constraints of HESS are as follows.

$$E^t_{H,ies} = \begin{cases} E^{t-1}_{H,ies} + \eta^{chr}_{H} Q^{t,ies}_{HESS,chr} & d^{t,ies}_{hess,chr} = 1 \\ E^{t-1}_{H,ies} + Q^{t,ies}_{HESS,dis} \Big/ \eta^{dis}_{H} & d^{t,ies}_{hess,dis} = 1 \end{cases} \tag{53}$$

$$E^1_H = E^T_H \tag{54}$$

$$0 \le E^t_H \le E^{\max}_H \tag{55}$$

$$\begin{cases} 0 \le Q^{t,ies}_{HESS,chr} \le Q^{\max}_{HESS} d^{t,ies}_{hess,chr} \\ 0 \le Q^{t,ies}_{HESS,dis} \le Q^{\max}_{HESS} d^{t,ies}_{hess,dis} \end{cases} \tag{56}$$

$$d^{t,ies}_{hess,chr} + d^{t,ies}_{hess,dis} \le 1 \tag{57}$$

where $E^t_{H,ies}$ denotes the amount of hydrogen stored in the HESS. $Q^{t,ies}_{HESS,chr}$ and $Q^{t,ies}_{HESS,dis}$ represent the hydrogen charging and discharging of the HESS. η^{chr}_H and η^{dis}_H correspond to the hydrogen charging and discharging efficiencies of the HESS, respectively. $d^{t,ies}_{hess,chr}$ and $d^{t,ies}_{hess,dis}$ represent the charging and discharging binary state coefficients of the HESS (with 0-1 variables), respectively. $Q^{\max}_{HESS}$ represents the maximum hydrogen charging and discharging of the HESS.

2) ENERGY BALANCE CONSTRAINS

The electrical balance constraints of IES are as follows.

$$E^{t,bef}_{load} + P^t_{AE} + P^t_{ES,chr} + \sum L^n_{ev} = P^t_{GT} + P^t_{ES,dis} + P^t_{buy} + P^t_{FC,ies} + P^t_{ies,c} \tag{58}$$

where: L^n_{ev} is the charging demand for regional EVs.

The heat balance constraints of IES are as follows.

$$H^{t,bef}_{load} + H^t_{HS,chr} = H^t_{GB} + H^t_{WHB} + H^t_{AE} + H^t_{HS,dis} + H^t_{FC,ies} \tag{59}$$

The hydrogen balance constraints of IES are as follows.

$$\sum L^n_{hev} + Q^{t,ies}_{HESS,chr} + Q^t_{FC,ies} = Q^t_{AE} + Q^{t,ies}_{HESS,dis} \tag{60}$$

where: L^n_{hev} is the hydrogen charging demand for regional HVs.

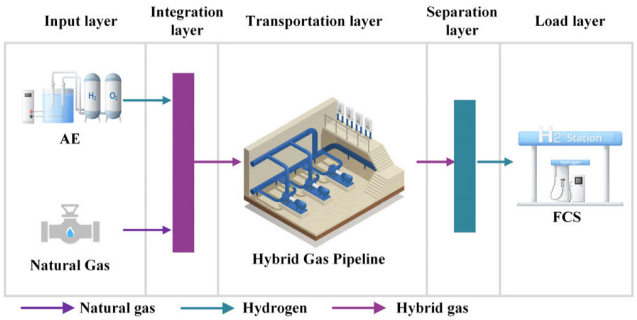

FIGURE 3. Schematic of shared natural gas pipeline transport.

3) SHARED NATRUAL GAS PIPELINE CONSTRAINS

It is possible to co-transporting hydrogen with natural gas through shared pipelines, which eliminates the need for dedicated hydrogen pipelines and fulfills the hydrogen demands of the related equipment [18]. Fig.3 illustrates this process, where hydrogen is separated using membrane separation equipment in the separation layer.

In order to determine the amount of the gas after the mixture of natural gas and hydrogen, as shown in the following formula:

$$Q_g^t = \sqrt{(Q_{g,gas}^t)^2 + (Q_{g,H}^t)^2} \tag{61}$$

where Q_g^t, $Q_{g,gas}^t$ and $Q_{g,H}^t$ represent the amount of mixed gas, natural gas, and hydrogen in the natural gas pipeline, respectively.

The hydrogen separation process incurs losses, as demonstrated by the subsequent formula.

$$Q_{ms}^t = \lambda_{ms} Q_{g,H}^t \tag{62}$$

where Q_{ms}^t is the amount of separated hydrogen. λ_{ms} is the hydrogen recovery rate (90%).

The constraint of the natural gas pipeline are as follows:

$$Q_{g,mb}^t = k_{mb} s_{mb}^t \sqrt{s_{mb}^t \left(p_{m,t}^2 - p_{b,t}^2\right)} \tag{63}$$

$$k_{mb} = \left(\frac{T_0 \times d_{mb}^5}{1.62 \times \rho \times T \times Z \times l_{mb} \times \lambda_{mb}} \right)^{0.5} \tag{64}$$

$$s_{mb}^t = \begin{cases} +1 & p_{m,t} \geq p_{b,t} \\ -1 & p_{m,t} \leq p_{b,t} \end{cases} \tag{65}$$

$$-Q_{g,mb}^{\max} \leq Q_{g,mb}^t \leq Q_{g,mb}^{\max} \tag{66}$$

where $Q_{g,mb}^t$ is the mixed gas flow in the pipeline. k_{mb} is the transmission coefficient of pipeline mb, which depends on the gas density, transport temperature, pipeline length, and pipeline inner diameter. s_{mb}^t is the flow-direction coefficient of the mixed gas in the pipeline. $p_{m,t}$ and $p_{b,t}$ are the gas pressures at pipeline nodes. $Q_{g,mb}^{\max}$ is the maximum transmission flow of the pipeline. The pipeline coefficient parameters can be found in [27].

III. SOLUTION METHODOLOGY

A. CARBON EMISSIONS CALCULATIONS

The primary providers to carbon emissions in the discussed IES are GT, GB, and the upper grid. Carbon emission intensity generally correlates with equipment power [25]. Therefore, the formula for carbon emissions conversion is as follows:

$$\begin{cases} D_{grid}^t = e_{grid} P_{grid}^t \\ D_{GT,e}^t = e_{GT} P_{GT}^t \\ D_{GT,h}^t = e_{GT} H_{GT}^t \\ D_{GB}^t = e_{GB} H_{GB}^t \end{cases} \tag{67}$$

$$EF_{ccer}^{IES} = \frac{D_{grid}^t + D_{GT,e}^t + D_{GT,h}^t + D_{GB}^t}{P_{grid}^t + P_{GT}^t + H_{GT}^t + H_{GB}^t} \tag{68}$$

where D_{grid}^t and D_{GB}^t represent the carbon emissions of the upper grid and the GB, respectively. $D_{GT,e}^t$ and $D_{GT,h}^t$ represent the carbon emissions from the GT for electricity generation and heat production, respectively. e_{grid} is the carbon emissions per unit of electricity supplied by the upper grid, which is taken as 0.728 kg/kWh. e_{GT} is the carbon emissions per unit of electricity generated by the GT, which is taken as 0.612 kg/kWh. e_{GB} represents the carbon emissions per unit of electricity generated by the GB, taken as 0.102 kg/kWh. EF_{ccer}^{IES} is the carbon emission coefficient per unit of electricity used by an IES.

Given the energy losses associated with energy storage and release in the ESS, this energy loss is defined as the carbon emission responsibility of the ESS. This can be expressed using the following formula:

$$D_{ES}^t = \begin{cases} (1 - \eta_{ES}^{chr}) P_{ES,chr}^t EF_{ccer}^{IES} & d_{es,chr}^t = 1 \\ \left(P_{ES,dis}^t \Big/ \eta_{ES}^{dis} - P_{ES,dis}^t \right) EF_{ccer}^{IES} & d_{es,dis}^t = 1 \end{cases} \tag{69}$$

where D_{ES}^t represent the carbon emissions from the ESS.

Reference [28] introduces a carbon emission flow model based on the PDN and used it to delineate the allocation of carbon emission responsibilities. It is important to note that this study did not account for carbon losses occurring in the PDN. Consequently, the carbon emission responsibilities of the nodes are contingent on their active power. The carbon emission density of the PDN is as follows:

$$\rho_{pdn}^t = \frac{D_{grid}^t + D_{GT,e}^t + D_{ES}^t}{\sum p_j^t} \tag{70}$$

B. LIFECYCLE CARBON EMISSION ASSESSMENT METHOD

Given that the planned equipment in EHIES are clean energy sources that do not emit carbon during the electricity generation, it is necessary to consider the lifecycle carbon emissions of these equipment. Lifecycle carbon emissions refer to the total carbon emissions generated by the equipment from production to disposal throughout their entire lifecycles. To address this concern, we employ the LCA method. Based

TABLE 2. The materials and corresponding carbon emissions for hydrogen energy equipment per unit capacity (kWh).

Equipment name	Material	Quantity(kg)	Emission factor($kgCO2_{eq}$/kg)
PEM electrolyzer	Unalloyed steel	4.57	1.51
	Stainless steel	0.37	4.85
	Copper	1.07	2.13
	Aluminium	0.33	9.5
	Titanium	0.17	46.5
	Polyethylene	0.12	2.28
FC	Cast iron	0.064	1.72
	Active carbon	0.02	0.21
	Polystyrene	0.24	3.69
	Stainless steel	0.6	4.85
	Aluminium	0.37	9.5
	Titanium	$5.6*10^{-3}$	46.5
HESS	Polyethylene	0.1	2.28
	Carbon powder	2.37	1.43
	Epoxy resin	0.35	2.04

TABLE 3. Energy required for the production of hydrogen energy equipment per unit capacity (kWh).

Energy types	Energy consumption	Emission factor
Electricity	25.32(kWh)	0.385 (kgCO2eq/kWh)
Diesel	1.64(L)	2.68 ($kgCO2_{eq}$/L)

on this method, we calculate the average daily carbon emissions of the equipment over their lifespans. In [29] and [30], it was noted that the unit electricity carbon emissions for the WT and PV were 0.038 kg/kWh and 0.0464 kg/kWh, respectively. The equation for calculating the lifecycle carbon emissions of WT and PV under ideal conditions is as follows:

$$LC_n = EF_n^e \cdot \beta_n N_n \quad n \in \{WT, PV\} \tag{71}$$

where EF_n^{re} represents the unit electricity carbon emissions for the WT and PV.

The materials and corresponding carbon emissions for hydrogen energy equipment per unit capacity are detailed in Table 2. Additionally, the energy consumption and corresponding carbon emissions for producing hydrogen energy equipment per unit capacity are provided in Table 3. The formula for calculating the lifecycle carbon emissions of hydrogen energy equipment is as follows:

$$LC_n = \left(\sum M_{n,k} \cdot EF_{n,k} + E_{em} \cdot EF_n^e\right) \beta_n N_n \quad n \in \{PEM, HESS, FC\} \tag{72}$$

where $M_{n,k}$ is the kth type of raw material for equipment. $EF_{n,k}$ represents the carbon emissions generated from the production of the kth type of raw material. E_{em} represents the energy consumed during production. EF_n^e represents the carbon emissions associated with this energy.

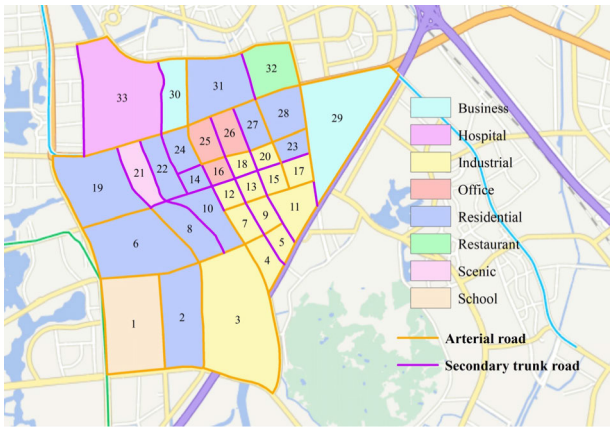

FIGURE 4. Functional zoning results and road grades.

C. PREDICTION OF EV CHARGING DEMAND AND HV HYDROGEN CHARGING DEMAND

The hydrogen charging requirements of HVs, which constitute a significant hydrogen load within the research area, exhibit spatiotemporal uncertainties [31]. Nonetheless, they share certain similarities with EV travel patterns. In this section, we model the travel behavior of both HVs and EVs by considering factors such as user travel patterns, traffic flow, and road classification. To predict regional electricity and hydrogen charging demands, we employed a Monte Carlo algorithm for the simulation. The geographical division of functional areas and classification of road classifications within the research area are illustrated in Fig. 4.

User travel patterns provide insights into the travel behaviors of various individuals. First, we classified users' travel destinations into five distinct categories: residential (H), work-related (W), shopping and dining (S), social and leisure activities (E), and miscellaneous (O), each associated with specific functional areas. We then establish a probability transition matrix to elucidate the likelihood of users moving from one destination to another, as shown in the following formula:

$$TP_{ij} = \begin{matrix} H \\ W \\ S \\ E \\ O \end{matrix} \begin{bmatrix} P_{11} & P_{21} & P_{31} & P_{41} & P_{51} \\ P_{12} & P_{22} & P_{32} & P_{42} & P_{52} \\ P_{13} & P_{23} & P_{33} & P_{43} & P_{53} \\ P_{14} & P_{24} & P_{34} & P_{44} & P_{54} \\ P_{15} & P_{25} & P_{35} & P_{45} & P_{55} \end{bmatrix} \tag{73}$$

$$0 \le TP_{ij} \le 1 \tag{74}$$

$$\sum_{j}^{5} TP_{ij} = 1 \quad i = 1, 2, \cdots, 5 \tag{75}$$

where TP_{ij} represents the probability of users transitioning from destination i to destination j.

This study classifies user travel patterns into two categories: simple and complex. Simple chains consist of two destination types, with residential area at both the start and end, while intermediate destination is chosen from other functional areas. Complex chains consist of three destination types, with residential area at both the start and end, and two

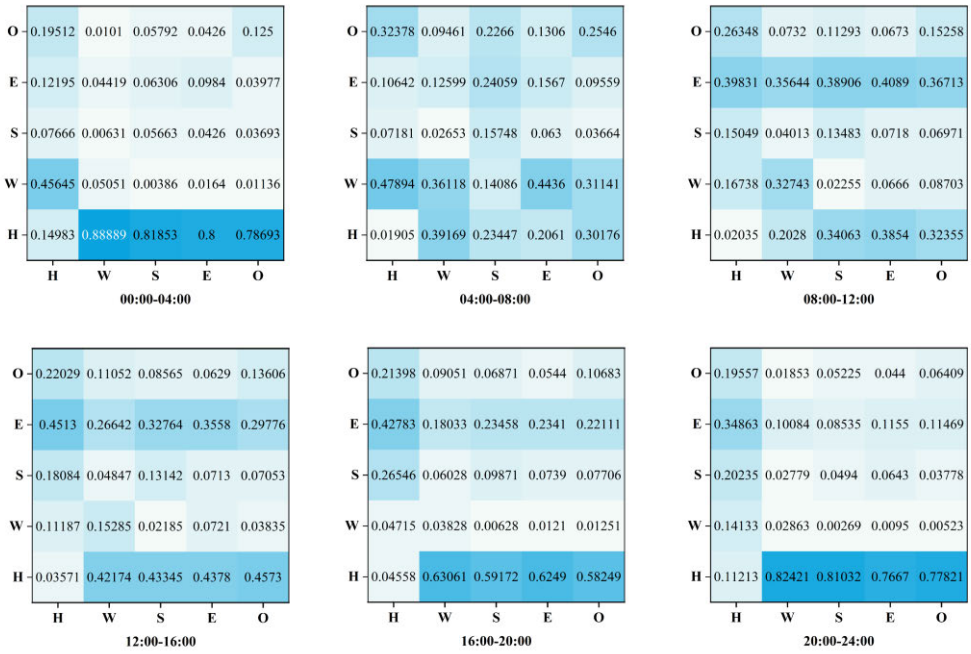

FIGURE 5. Transition probabilities for the six time periods.

intermediate destinations chosen from other functional areas. The day is segmented into six time periods, and the likelihood of users selecting functional areas varied across these periods. Consequently, the transition probabilities are derived from the data in reference [32], as illustrated in Fig. 5.

In the daily commuting routines of private car owners, EV users commonly choose to charge their vehicles at charging piles near parking lots or utilize FCS for urgent charging. In order to minimize battery loss as much as possible, private car owners frequently prefer slow charging at night. By contrast, HV users only rely on FCS for refueling. According to [33], the daily start times for private car users conform to a normal distribution $N(8.56, 1.572)$. The durations of activities related to leisure and work follow normal distributions, $N(2.39, 0.732)$ and $N(5.87, 1.22)$, respectively. Meanwhile, the durations of activities such as resting at home, shopping, and other miscellaneous activities adhere to exponential distributions $E(2.28)$, $E(0.56)$, and $E(0.45)$, respectively.

Given that vehicle energy consumption primarily depends on driving speed, which is in turn influenced by road classifications and traffic flow, we formulate the equations for EV driving speed V_{ev} and energy consumption e^t_{ev} as follows:

$$R = m + \eta\left(\frac{L_k^{Cap,t}}{L_k^{Cap,\max}}\right)^3 \tag{76}$$

$$V^t_{L_k} = \frac{v^{rl} \cdot (L_k^{Cap,\max})^R}{1 + L_k^{Cap,t}} \tag{77}$$

$$e^t_{ev} = 0.21 - 0.001V^t_{L_k} + \frac{1.531}{V^t_{L_k}} \tag{78}$$

where v^{rl} is the maximum driving speed for the different road classifications (rl=1, 2). R is the road capacity coefficient. $L_k^{Cap,t}$ and $L_k^{Cap,\max}$ represent the actual traffic capacity and road capacity of road segment L_k in time period t, respectively. $V^t_{L_k}$ is the driving speed of vehicles on road segment L_k at time t.

Utilizing HV data supplied by the BIG HIT project [34], we formulate the driving energy consumption model as follows:

$$e^t_{hev} = \lambda_{hev} V^t_{L_k} \cdot \Delta t \tag{79}$$

where e^t_{hev} denotes the driving energy consumption of the HV. λ_{hev} is the energy consumption coefficient.

Finally, it is specified that upon reaching their destination, if an EV remains stationary for more than 10 minutes with a state of charge (SOC) below the charging threshold, charging is initiated. In the case of an HV, when the SOC falls below the hydrogen replenishment threshold, the vehicle will proceed to a FCS for hydrogen replenishment. Once the charging behavior of EV and HV users is confirmed, the simulation algorithm updates the charging load L^n_{ev} for different functional zones within the planning area and the hydrogen energy load L^n_{hev} for FCS in accordance with the provided logic. The simulation algorithm runs in the MATLAB r2023a environment, and its workflow is illustrated in Figure 6.

D. TWO-STAGE COORDINATED PLANNING METHOD

The planning problem for the EHIES is structured in two distinct stages. The first stage involves the EHIES planning, while the second stage focuses on simulating EHIES operations to provide low-carbon energy, thereby reducing system carbon emissions for IES. An overview of the solution process is shown in Fig. 7.

In the first stage, as it involves mixed integer nonlinear programming, we employ the commercial solver Gurobi

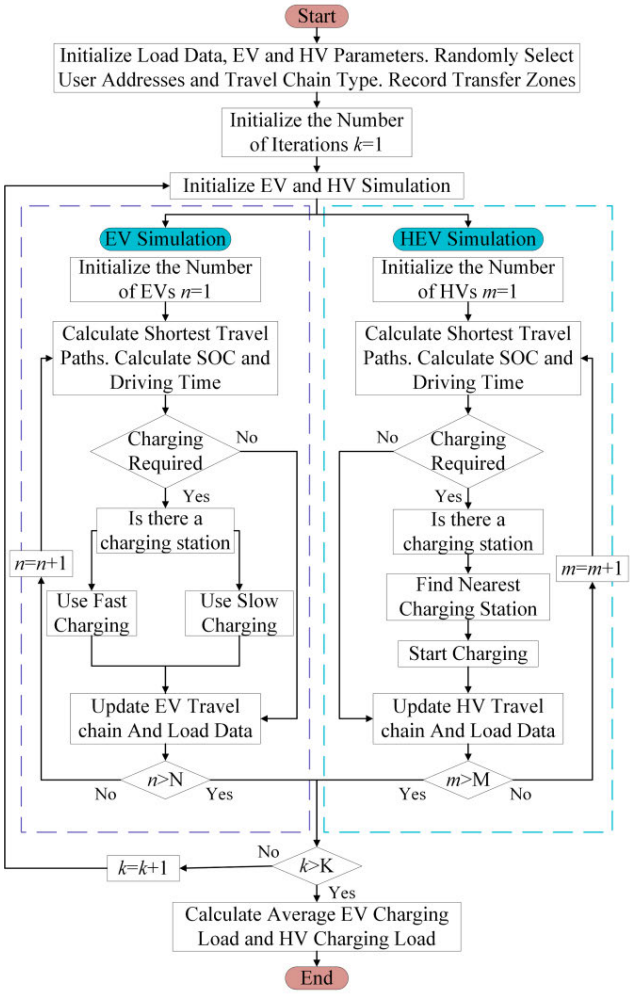

FIGURE 6. Simulation algorithm workflow diagram.

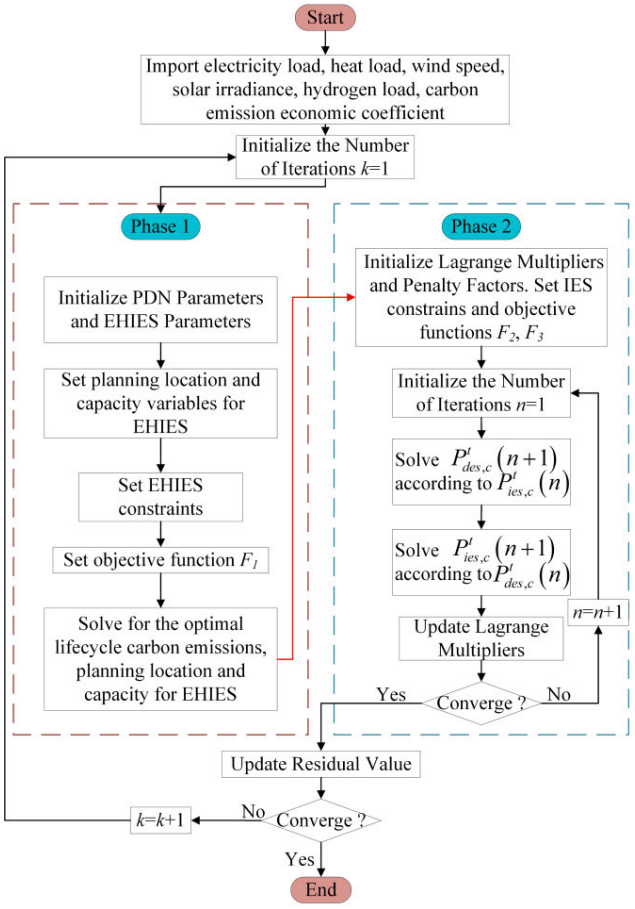

FIGURE 7. Flowchart of the two-stage planning method.

9.1 through the Yalmip tool within the MATLAB r2023a environment to obtain solutions. Following this, we establish a distributed optimization framework for managing outputs when the EHIES is connected to the IES, guided by the second-stage objective function. In this context, we choose the ADMM, a straightforward, efficient, and robust algorithm that does not require a strictly convex optimization problem. To solve the objective function, the power generation of the EHIES to IES serves as a coupling variable, and its formula is as follows:

$$\begin{aligned} &F_2 + F_3 \\ &s.t.\ \ P^t_{ies,c} - P^t_{des,c} = 0 \end{aligned} \tag{80}$$

Then, construct the following augmented Lagrangian function:

$$\begin{aligned} \min L_\rho = F_2 + F_3 + \sum_t^{24} \Big[& u^T \left(P^t_{ies,c} - P^t_{des,c} \right) \\ & + \frac{\rho}{2} \left\| P^t_{ies,c} - P^t_{des,c} \right\|_2^2 \Big] \end{aligned} \tag{81}$$

where u^T represents the Lagrange multiplier coefficient. ρ represents the penalty factor.

The iterative calculation steps are as follows:

$$\begin{cases} P^t_{des,c}(\omega+1) = \arg\min L_\rho \left[P^t_{des,c}(\omega), P^t_{ies,c}(\omega), u^T(\omega) \right] \\ P^t_{ies,c}(\omega+1) = \arg\min L_\rho \\ \left[P^t_{des,c}(\omega+1), P^t_{ies,c}(\omega), u^T(\omega) \right] \\ u^T(\omega+1) = u^T(\omega) + \rho \left[P^t_{ies,c} - P^t_{des,c} \right] \end{cases} \tag{82}$$

$$\begin{aligned} err = & \sum \left\| P^t_{des,c}(\omega+1) - P^t_{des,c}(\omega) \right\|_2 \\ & + \sum \left\| P^t_{ies,c}(\omega+1) - P^t_{ies,c} \right\|_2 \le \varepsilon \end{aligned} \tag{83}$$

where ω is the number of iterations required to solve the sub-problem to minimize the objective function. err is the dual residual. ε is the convergence value of the dual residuals.

After obtaining the optimal EHIES to IES power generation, it is substituted as a constraint in the first stage. The additional constraint formula is as follows:

$$E^{t,0}_{load} + P^t_{PEM} + P^t_{des,c}(\omega^*) \le P^t_{PV} + P^t_{WT} + P^t_{FC,des} \tag{84}$$

where $P^t_{des,c}(\omega^*)$ represents the optimal power generation of EHIES to IES.

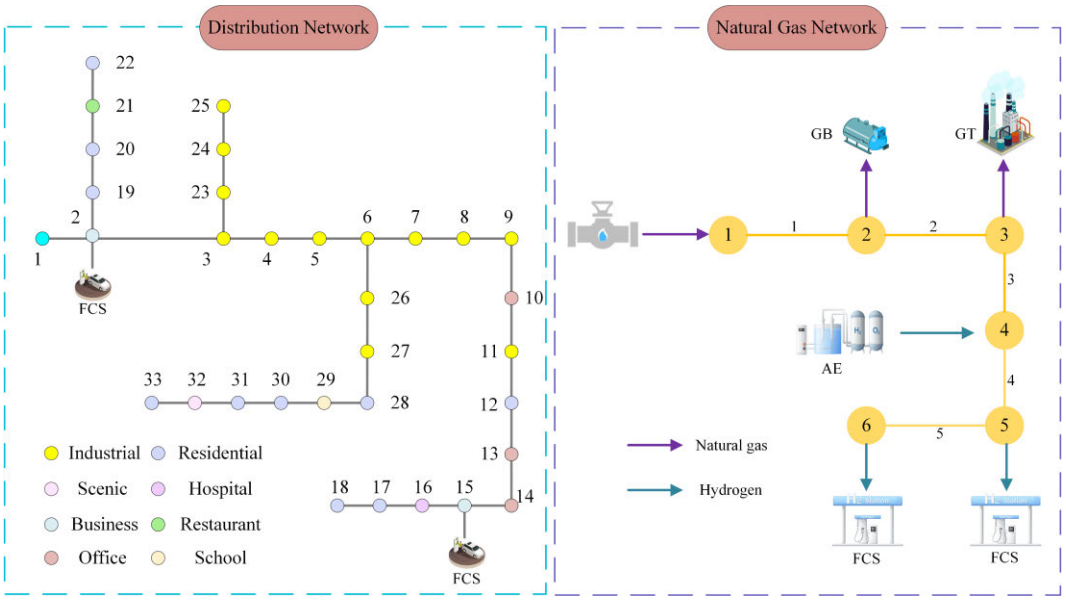

FIGURE 8. Network topology diagram.

Considering that the constraints of PDN and natural gas network are nonlinear, the second-order cone relaxation method in [18] is applied. In this paper, the Yalmip tool is employed to model and invoke the commercial solver Gurobi 9.1 to solve the problems in the MATLAB r2023a environment.

IV. CASE STUDIES

A. TEST SYSTEM DESCRIPTION

This study analyzes the improved IEEE 33-bus PDN [18] and 6-node natural gas network [35], as shown in Fig. 8. The FCSs are connected to nodes 2 and 15 of the PDN. In the natural gas network, node 1 is the supply node of the natural gas supplier, node 2 connects to the GB, node 3 connects to the GT, node 4 acts as the access node for the AE to supply hydrogen. Nodes 5 and 6 are the access nodes for hydrogen charging. Nodes 1 and 4 maintain a gas pressure range of [5] and [6] Mpa, while the other nodes operate within a range of [3] and [7] Mpa, as detailed in Table 4. IEEE 33-bus power node corresponding functional area numbers are presented in Table 5. The parameters of the system access equipment of node 1 where the IES connects to the PDN, are listed in Table 6. Considering the uncertainty of wind speed and solar irradiance input data, the selected range values are shown in Fig. 9. v_{ci}, v_{ra}, v_{out}, and η_{PV} are 2.5, 7, 9 and 0.001. The service life of WT and PV is 20 years. The prices of the upper grid and natural gas are derived from the real-time wholesale market prices, as depicted in Figure 10. The heating value of natural gas is 12.125 kWh/kg. The carbon emission economic coefficient is 0.12 CNY/kg. The parameters of the various devices in the EHIES are shown in Table 7. The scheduling cycle for the system spans one day, t=24 h, with 1-hour scheduling intervals. The electric and heat load in this area is shown in Fig. 11 (a). When there is a demand for hydrogen charging for HVs in the area, they visit the HCS, also known as FCS. The hydrogen charging load of the HCS is displayed in Fig. 11 (b). EVs in the region decide whether to charge slowly or quickly, based on their specific locations. The charging load connected to the PDN is illustrated in Fig. 11 (c). The active loads of PDN nodes corresponding to different functional areas are shown in Fig. 11 (d).

TABLE 4. Natural gas pipeline parameters.

Pipeline number	Start node	End node	Diameter(m)	Length(m)
1	1	2	0.9	500
2	2	3	0.9	400
3	3	4	0.9	300
4	4	5	0.9	400
5	5	6	0.9	429

TABLE 5. IEEE 33-bus power node corresponding functional area numbers.

Node number	Function zone number	Node number	Function zone number	Node number	Function zone number
2	29	13	16	24	20
3	11	14	25	25	27
4	15	15	30	26	4
5	5	16	33	27	3
6	7	17	24	28	2
7	9	18	22	29	1
8	13	19	23	30	6
9	18	20	28	31	19
10	26	21	32	32	21
11	12	22	31	33	8,10
12	14	23	17		

B. EFFECTIVENESS OF COLLABORATIVE PLANNING STRATEGE

To explore the influence of low-carbon power supplied by an EHIES on IES in terms of planning outcomes and car-

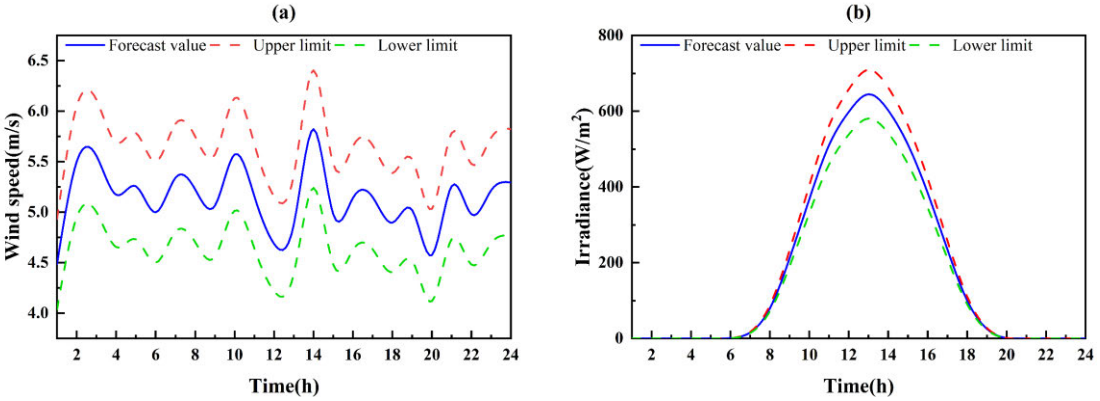

FIGURE 9. Input data: (a) Wind speed input data. (b) Solar irradiance input data.

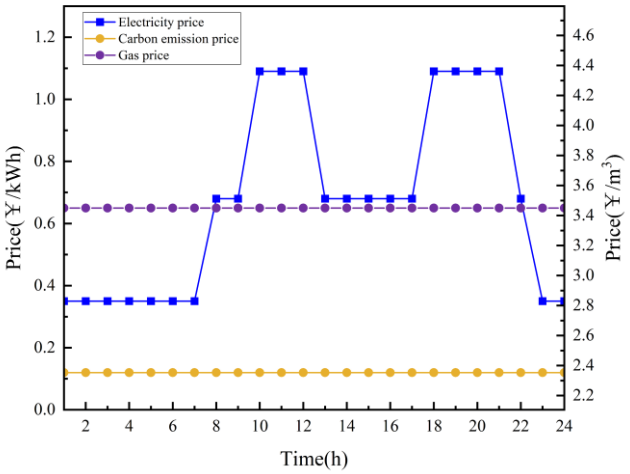

FIGURE 10. Energy price analysis chart.

bon emissions, this study established two distinct simulation scenarios: one for independent operation and the other for coordinated operation.

Scenario 1: This scenario focuses on EHIES planning, considering only the investment costs and their implications for active network losses and voltage deviation within the distribution network.

Scenario 2: In this scenario, EHIES planning is extended to encompass the influence of EHIES generation on IES carbon emissions. The low-carbon electricity provided by EHIES to IES is coordinated optimized using the ADMM algorithm.

Scenario 3: This scenario focuses on DES (only PV and WT) planning, considering only the investment costs and their implications for active network losses and voltage deviation within the distribution network.

Scenario 4: This scenario uses the planning results of Scenario 2. The low-carbon electricity provided by EHIES to IES is optimized using the Big-M method.

Scenario 5: This scenario uses the planning results of Scenario 2. In the second stage, carbon emission responsibility is not considered and EHIES does not provide low-carbon electricity to IES.

Fig. 12 presents the iterative convergence results for Scenario 2. The graph on the left shows the convergence achieved after 31 iterations, while the graph on the right illustrates

TABLE 6. Parameters of system access equipment.

Equipment name	Installed capacity (kWh)	Operation costs (CNY)	Parameters	Numerical values
GT	2000	4.19	η_{GT}	0.8
			λ_{GT}	0.65
WHB	1000	7.22	λ_{re}	0.85
GB	1000	1.4	λ_{GB}	0.8
AE	600	3.75	q_{H_2}	39.4
			$\eta_{AE,e}$	0.6
			$\eta_{AE,h}$	0.88
PEM electrolyzer	42	3.75	η_{PEM}	0.57
ESS	1000	1.04	$\eta_{ES}^{chr}/\eta_{ES}^{dis}$	0.95
HSS	1000	0.36	$\eta_{HS}^{chr}/\eta_{HS}^{dis}$	0.92
HESS	1000	1.04	$\eta_{H}^{chr}/\eta_{H}^{dis}$	0.98
			$\lambda_{hess}^{\min},\lambda_{hess}^{\max}$	0.2,0.85
FC	100	2.95	λ_{FC}	3.04
			$\eta_{FC,e},\eta_{FC,h}$	0.6, 0.88

TABLE 7. Parameters of EHIES access equipment.

Equipment name	c_n (CNY/kWh)	β_n (10^{-4})	Max capacity (kWh)	Operation costs (CNY)
WT	4500	1.37	300	5.78
PV	3600	1.37	300	5.1378
PEM electrolyzer	2000	2.74	42	3.75
HESS	3000	2.74	460	1.04
FC	4000	2.74	200	2.95

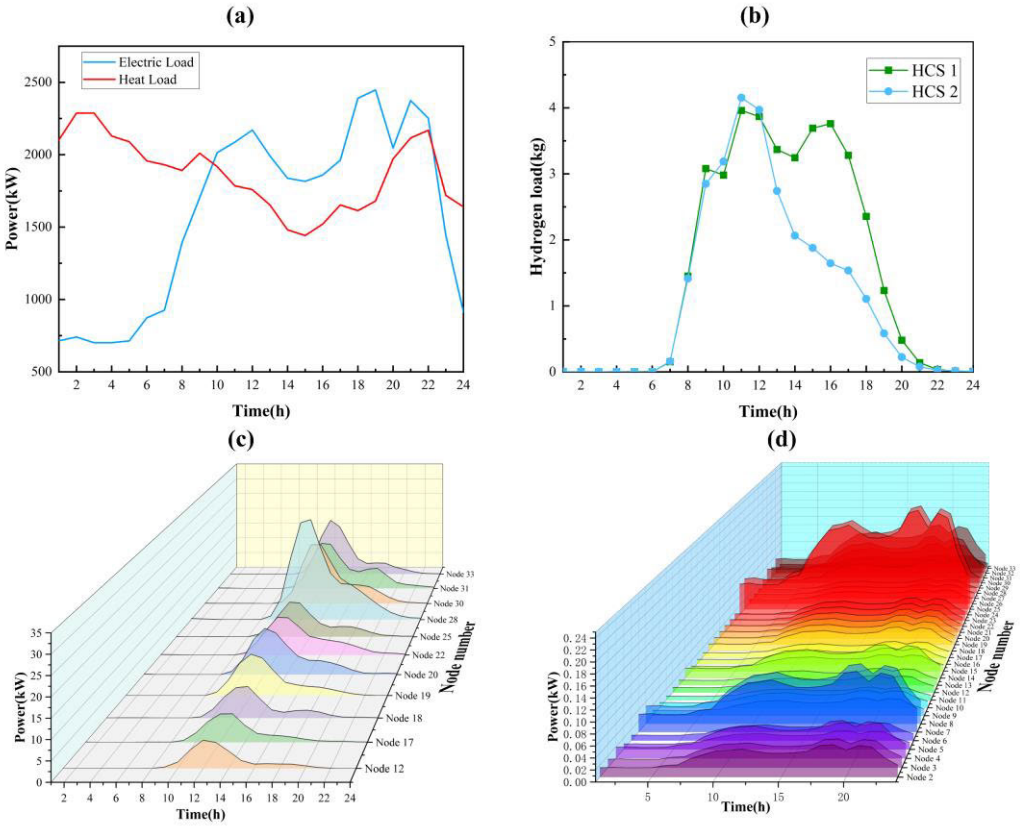

FIGURE 11. Regional load chart: (a) Electric and heat load data. (b) Forecasted hydrogen charging load for charging stations. (c) Forecasted electric vehicle charging load. (d) Electric load connected to the distribution network.

the status of the ADMM iterations at the final iteration. This iteration, the ADMM achieved convergence in 14 iterations.

The planning location and capacity results for the EHIES are listed in Table 8. The capacity of the EHIES in Scenario 1 is smaller than that in Scenario 2, therefore, its active network losses are smaller. The voltage deviation in Scenario 2 is slightly lower than that in Scenario 1, and the capacity configuration of the EHIES is more conducive to the voltage quality of the PDN and the service life of the equipment. Although the investment cost in Scenario 2 is higher than in Scenario 1, the lifecycle operating cost in Scenario 2 is significantly lower than this in Scenario 1. Compared to upfront investment costs, operating costs should not be underestimated. Compared to Scenario 1, Scenario 3 has significantly higher active power losses due to the absence of a hydrogen energy system. Additionally, both the investment cost and lifecycle operation and maintenance cost are higher than those in Scenario 1.

Figure 13 illustrates the carbon emissions and operating costs of the IES across five scenarios. It is evident that Scenario 2 exhibits the lowest carbon emissions and operating costs, whereas Scenario 1 demonstrates the highest carbon emissions, and Scenario 3 incurs the highest operating costs. Comparing Scenarios 1 and 2, it is apparent that Scenario 2's carbon emissions are significantly lower due to its consideration of lifecycle carbon emissions. In Scenario 5, the neglect of low-carbon electricity supply has led to increased IES carbon emissions. Furthermore, a comparison between Scenarios 2 and 4 reveals that the ADMM algorithm produces superior optimization results compared to the Big-M method.

Figure 14 presents the distribution of low-carbon electricity supply across three distinct scenarios. The lowest supply of low-carbon electricity is observed in Scenario 1. In Scenario 4, the supply is lower than in Scenario 1 at 20:00 and 23:00. Conversely, Scenario 2 demonstrates a higher supply compared to Scenario 1. Thus, it is evident that Scenario 2 yields better results in providing low-carbon electricity.

TABLE 8. Capacity planning results.

No	Scenario 1	Scenario 2	Scenario 3
Access node	28	17	18
WT (kW)	147	300	162
PV (kW)	53	145	50
HESS (kg)	51	173	-
FC (kW)	9	11	-
Active network loss (p.u.)	0.052	0.067	0.077
Voltage deviation (p.u.)	29.85	27.47	27.41
Investment cost (10^6 CNY)	1.125	2.519	1.242
Lifecycle Operating cost (10^6 CNY)	191.667	184.367	200.173

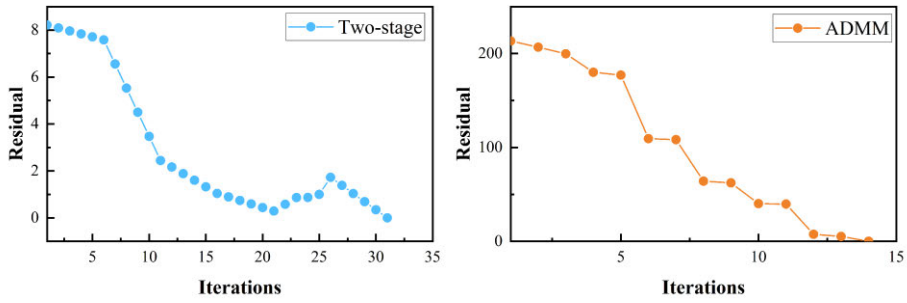

FIGURE 12. Iterative convergence.

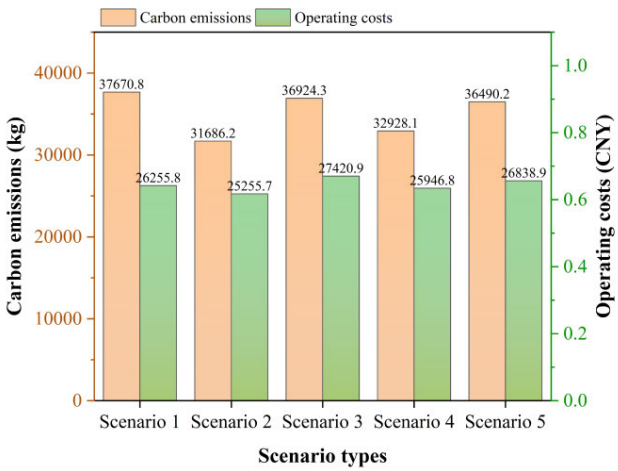

FIGURE 13. Comparison of optimization results.

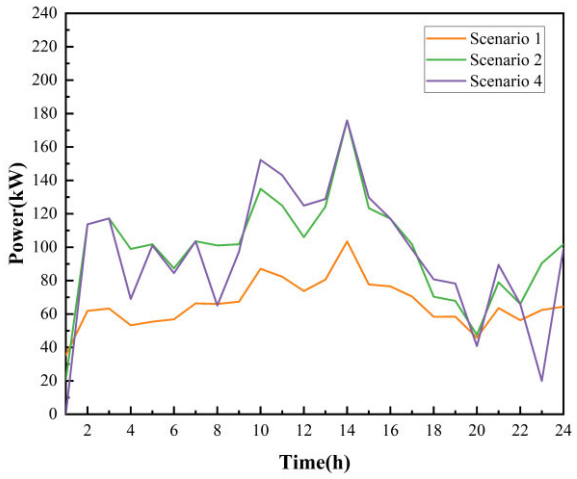

FIGURE 14. Power provided by EHIES to IES.

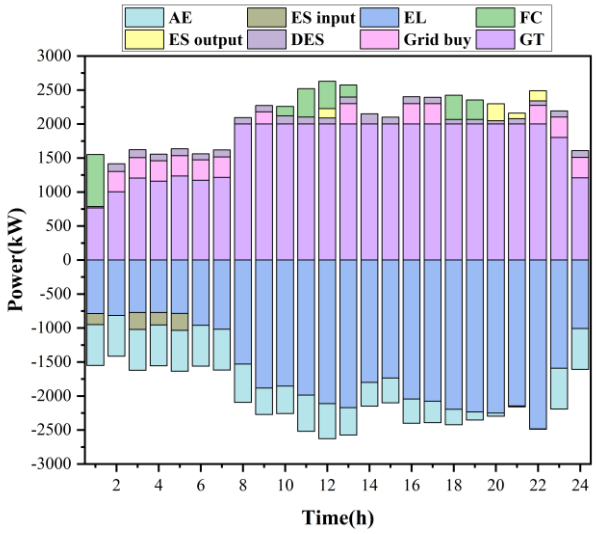

FIGURE 15. Illustrates the optimization results for the electrical system.

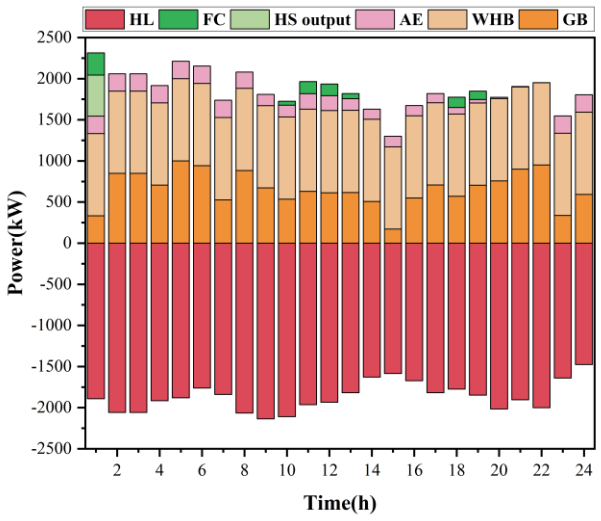

FIGURE 16. Displays the optimization results for the thermal system.

The electrical system of the IES established in this study consists mainly of GT, FC, AE, ESS, and EHIES. The thermal system includes the GB, WHB, HSS, AE, and FC. The optimization outcomes for the electrical and thermal systems in Scenario 2 are shown in Fig. 15. and Fig. 16.

Fig. 15. and Fig. 16. reveal the optimization results in Scenario 2. During this scenario, the AE operates at maximum capacity primarily during off-peak hours, from 23:00

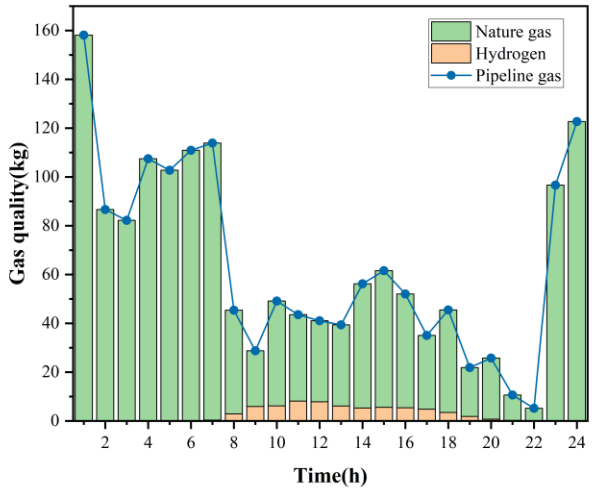

FIGURE 17. Gas balance in pipeline 3-5.

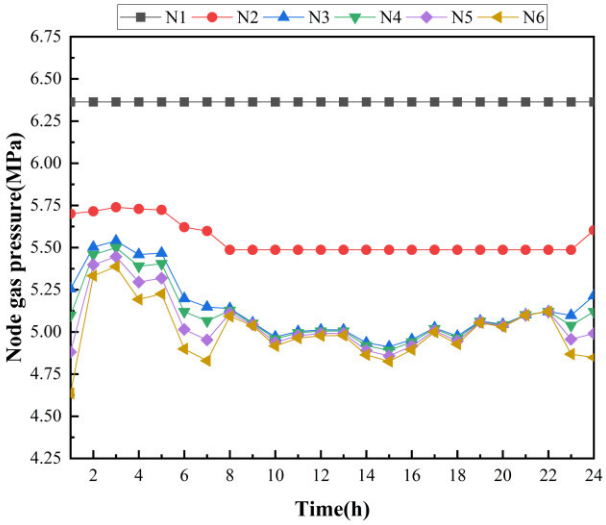

FIGURE 18. Gas pressure at different nodes in the pipeline.

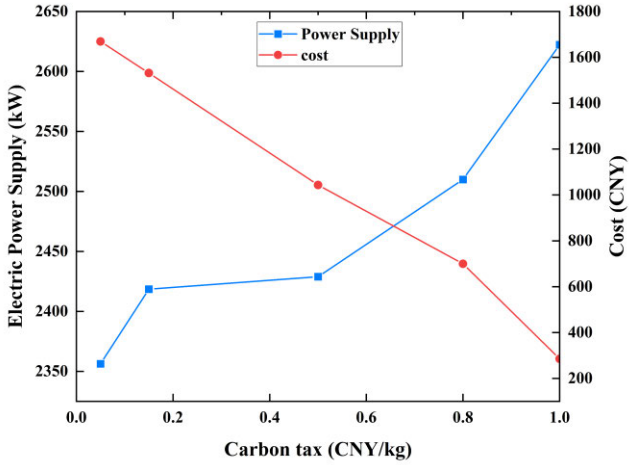

FIGURE 19. Power supply under different carbon tax prices.

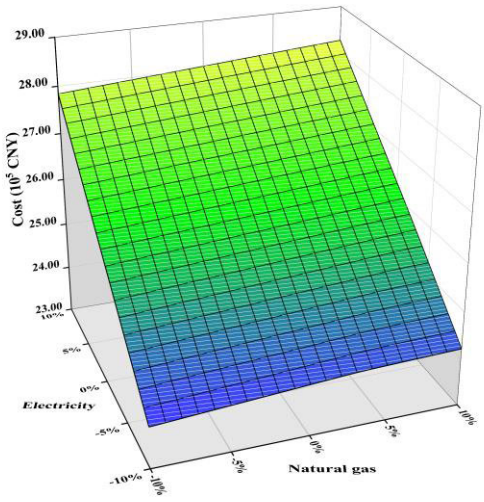

FIGURE 20. Operation costs with different market prices.

to 7:00. Hydrogen production gradually scales down from 8:00 to 22:00 as electricity prices increase. When hydrogen production by AE exceeds consumption by FC, the HESS initiates hydrogen replenishment. Surplus hydrogen is then transported via pipelines to the FCS to meet regional hydrogen demand, concurrently generating revenue for the system. Notably, FC power generation is predominantly concentrated during peak electricity demand hours, utilizing hydrogen from the HESS to meet regional electricity demand and offsetting power supply deficiencies when the GT output is low.

Pipeline 3-5 are used to deliver hydrogen from the hydrogen energy system to the FCS. The gas balance within the pipeline is depicted in Fig. 17. As Fig. 18. illustrates, during gas transportation, the pressure between the nodes gradually decreases while remaining well within the safe pressure range. This validates the safety of hydrogen supply within the system.

C. SENSITIVITY ANALYSIS

The carbon tax price affects the electricity supply and costs provided by EHIES to IES. As shown in Fig. 19, the electricity supplied by EHIES to IES varies at different carbon tax prices. It can be observed from the figure that the supply of electricity from EHIES to IES increases with the increase in carbon tax prices. Increasing the supply of electricity can result in economic subsidies, thereby reducing the economic costs of EHIES.

The operation of IES is influenced by the market prices of electricity and natural gas. Fig. 20 shows the impact of fluctuations in electricity and natural gas market prices within $\pm 10\%$ range on the economic cost of IES. It can be observed that the fluctuation in electricity market prices has a significantly higher impact on the system's economic cost compared to natural gas fluctuations.

Finally, the stochastic variations of solar and wind energy are crucial factors affecting HEIES. Table 9 displays the operational costs of both EHIES and DES (only PV and WT)

TABLE 9. Comparison of operating costs between EHIES and DES under different randomness.

Increment	Operating costs of EHIES (CNY)	Operating costs of DES (CNY)	Reduction ratio
5%	27314.94	27957.95	2.23%
10%	26326.12	27098.28	2.85%
15%	26005.85	26917.81	3.39%
20%	26426.88	27008.97	2.16%

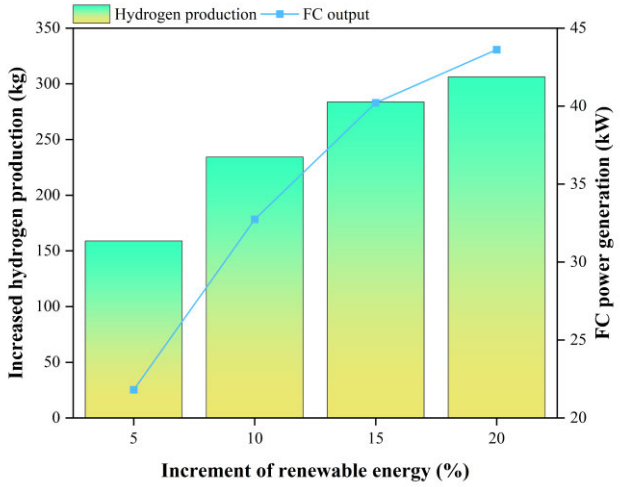

FIGURE 21. The hydrogen increment and FC output of the hydrogen energy system under various increments of renewable energy.

under different levels of randomness. It can be observed that the operating costs of EHIES under different levels of randomness are lower than DES without hydrogen equipment. The incorporation of hydrogen equipment enables the utilization of surplus energy from renewable sources, consequently reducing the operating costs of DES.

Given that hydrogen equipment utilizes surplus energy for hydrogen production, the discussion is confined to scenarios involving an increase in renewable energy. Fig. 21 illustrates the hydrogen increment and FC output of the hydrogen energy system under various increments of renewable energy. The figure shows a noticeable rise in both hydrogen increment and FC output with the increasing levels of renewable energy.

V. CONCLUSION

This paper presents a coordinated planning methodology for EHIES that considerations of lifecycle carbon emissions. Comparative scenario analysis involves two scenarios: independent and coordinated operations. Analysis of the objective function results, carbon emissions, and equipment operation led to three key conclusions:

(1) The EHIES model significantly enhances the efficient utilization of clean energy resources. In scenarios with surplus renewable energy, excess electricity can be converted to hydrogen using PEM electrolyzer and stored in the HESS. This surplus electricity is then transmitted through the PDN to the IES, reducing the IES output and operating cost of the system. This in turn improves the economic efficiency of IES operations.

(2) During the planning phase, considering the lifecycle carbon emissions of the EHIES equipment allows for the effective quantification of unit power carbon emissions from clean energy devices over their entire lifecycle. This enables a more robust system operational strategy design, leading to reduced overall carbon emissions.

(3) The inclusion of coordinated operation between the EHIES and IES in the second planning stage effectively reduces the total operating costs and carbon emissions of the system. The EHIES benefits from additional revenue through carbon emission subsidies provided by the IES, based on its contributions. In the results analysis section, the coordinated planning approach reduces the total operating costs by 3.81% and carbon emissions by 15.89%.

This paper investigates the impact of coordinated planning EHIES, considering lifecycle carbon emissions. However, the uncertainty in the source and load may also influence the supply of energy between devices in EHIES. If a more accurate modeling of source and load uncertainty is considered during the planning, it could lead to better planning outcomes. Furthermore, this study only takes into account constraints related to the transmission of hydrogen and natural gas using natural gas pipelines after their mixture. The coupling of PDN and natural gas pipelines with a strategy for joint operation using electricity to hydrogen conversion remains to be explored in further research. Some researchers have considered the impact of extreme events when planning the system [36]. In planning hydrogen energy systems, it is possible to increase consideration of the performance of hydrogen equipment in extreme situations, utilizing hydrogen equipment to mitigate the impact of extreme conditions on the IES.

REFERENCES

[1] T. Egeland-Eriksen, A. Hajizadeh, and S. Sartori, "Hydrogen-based systems for integration of renewable energy in power systems: Achievements and perspectives," *Int. J. Hydrogen Energy*, vol. 46, no. 63, pp. 31963–31983, Sep. 2021, doi: 10.1016/j.ijhydene.2021.06.218.

[2] L. Liu and Z. Qin, "Low-carbon planning for park-level integrated energy system considering optimal construction time sequence and hydrogen energy facility," *Energy Rep.*, vol. 9, pp. 554–566, Sep. 2023, doi: 10.1016/j.egyr.2023.04.208.

[3] A. Kovac, M. Paranos, and D. Marcius, "Hydrogen in energy transition: A review," *Int. J. Hydrogen Energy*, vol. 46, no. 16, pp. 10016–10035, Mar. 2021, doi: 10.1016/j.ijhydene.2020.11.256.

[4] S. Basnet, K. Deschinkel, L. Le Moyne, and M. Cécile Péra, "A review on recent standalone and grid integrated hybrid renewable energy systems: System optimization and energy management strategies," *Renew. Energy Focus*, vol. 46, pp. 103–125, Sep. 2023, doi: 10.1016/j.ref.2023.06.001.

[5] Y. Song, H. Mu, N. Li, and H. Wang, "Multi-objective optimization of large-scale grid-connected photovoltaic-hydrogen-natural gas integrated energy power station based on carbon emission priority," *Int. J. Hydrogen Energy*, vol. 48, no. 10, pp. 4087–4103, Feb. 2023, doi: 10.1016/j.ijhydene.2022.10.121.

[6] Y. Jiao and D. Månsson, "Greenhouse gas emissions from hybrid energy storage systems in future 100% renewable power systems—A Swedish case based on consequential life cycle assessment," *J. Energy Storage*, vol. 57, Jan. 2023, Art. no. 106167, doi: 10.1016/j.est.2022.106167.

[7] L. de Oliveira-Assis, P. García-Triviño, E. P. P. Soares-Ramos, R. Sarrias-Mena, C. A. García-Vázquez, C. E. Ugalde-Loo, and L. M. Fernández-Ramírez, "Optimal energy management system using bio-geography based optimization for grid-connected MVDC microgrid with photovoltaic, hydrogen system, electric vehicles and Z-source converters," *Energy Convers. Manag.*, vol. 248, Nov. 2021, Art. no. 114808, doi: 10.1016/j.enconman.2021.114808.

[8] N. Huang, X. Zhao, Y. Guo, G. Cai, and R. Wang, "Distribution network expansion planning considering a distributed hydrogen-thermal storage system based on photovoltaic development of the whole county of China," *Energy*, vol. 278, Sep. 2023, Art. no. 127761, doi: 10.1016/j.energy.2023.127761.

[9] A. H. Schrotenboer, A. A. T. Veenstra, M. A. J. U. H. Broek, and E. Ursavas, "A green hydrogen energy system: Optimal control strategies for integrated hydrogen storage and power generation with wind energy," *Renew. Sustain. Energy Rev.*, vol. 168, Oct. 2022, Art. no. 112744, doi: 10.1016/j.rser.2022.112744.

[10] X. Dong, J. Wu, Z. Xu, K. Liu, and X. Guan, "Optimal coordination of hydrogen-based integrated energy systems with combination of hydrogen and water storage," *Appl. Energy*, vol. 308, Feb. 2022, Art. no. 118274, doi: 10.1016/j.apenergy.2021.118274.

[11] Y. Wang, C. Liu, Y. Qin, Y. Wang, H. Dong, Z. Ma, and Y. Lin, "Synergistic planning of an integrated energy system containing hydrogen storage with the coupled use of electric-thermal energy," *Int. J. Hydrogen Energy*, vol. 48, no. 40, pp. 15154–15178, May 2023, doi: 10.1016/j.ijhydene.2022.12.334.

[12] Y. Wang, F. Huang, S. Tao, Y. Ma, Y. Ma, L. Liu, and F. Dong, "Multi-objective planning of regional integrated energy system aiming at exergy efficiency and economy," *Appl. Energy*, vol. 306, Jan. 2022, Art. no. 118120, doi: 10.1016/j.apenergy.2021.118120.

[13] Y. Dong, Z. Han, C. Li, S. Ma, and Z. Ma, "Research on the optimal planning method of hydrogen-storage units in wind–hydrogen energy system considering hydrogen energy source," *Energy Rep.*, vol. 9, pp. 1258–1264, Oct. 2023, doi: 10.1016/j.egyr.2023.05.116.

[14] T. Bragatto, F. Carere, M. Cresta, F. M. Gatta, A. Geri, V. Lanza, M. Maccioni, and M. Paulucci, "Location and sizing of hydrogen based systems in distribution network for renewable energy integration," *Electric Power Syst. Res.*, vol. 205, Apr. 2022, Art. no. 107741, doi: 10.1016/j.epsr.2021.107741.

[15] Z. Zheng, T. Liu, Q. Liu, J. Lei, and J. Fang, "A distributed energy system integrating SOFC-MGT with mid-and-low temperature solar thermochemical hydrogen fuel production," *Int. J. Hydrogen Energy*, vol. 46, no. 38, pp. 19846–19860, Jun. 2021, doi: 10.1016/j.ijhydene.2021.03.137.

[16] E. Gul, G. Baldinelli, A. Farooqui, P. Bartocci, and T. Shamim, "AEM-electrolyzer based hydrogen integrated renewable energy system optimisation model for distributed communities," *Energy Convers. Manag.*, vol. 285, Jun. 2023, Art. no. 117025, doi: 10.1016/j.enconman.2023.117025.

[17] S. Jafarpour and M. H. Amirioun, "A resilience-motivated restoration scheme for integrated electricity and natural gas distribution systems using adaptable microgrid formation," *IET Gener., Transmiss. Distribution*, vol. 17, no. 23, pp. 5223–5239, Dec. 2023, doi: 10.1049/gtd2.13032.

[18] J. Ding, C. Gao, M. Song, X. Yan, and T. Chen, "Optimal operation of multi-agent electricity-heat-hydrogen sharing in integrated energy system based on Nash bargaining," *Int. J. Electr. Power Energy Syst.*, vol. 148, Jun. 2023, Art. no. 108930.

[19] Y.-J. Zhang, T. Liang, Y.-L. Jin, and B. Shen, "The impact of carbon trading on economic output and carbon emissions reduction in China's industrial sectors," *Appl. Energy*, vol. 260, Feb. 2020, Art. no. 114290, doi: 10.1016/j.apenergy.2019.114290.

[20] R. Tan and B. Lin, "The long term effects of carbon trading markets in China: Evidence from energy intensive industries," *Sci. Total Environ.*, vol. 806, Feb. 2022, Art. no. 150311, doi: 10.1016/j.scitotenv.2021.150311.

[21] Y. Li, F. Bu, J. Gao, and G. Li, "Optimal dispatch of low-carbon integrated energy system considering nuclear heating and carbon trading," *J. Cleaner Prod.*, vol. 378, Dec. 2022, Art. no. 134540, doi: 10.1016/j.jclepro.2022.134540.

[22] R. Wang, L. Yang, X. Wang, and Y. Zhou, "Low carbon optimal operation of integrated energy system based on concentrating solar power plant and power to hydrogen," *Alexandria Eng. J.*, vol. 71, pp. 39–50, May 2023, doi: 10.1016/j.aej.2023.03.038.

[23] L. Wang, Z. Tao, L. Zhu, X. Wang, C. Yin, H. Cong, R. Bi, and X. Qi, "Optimal dispatch of integrated energy system considering integrated demand response resource trading," *IET Gener., Transmiss. Distrib.*, vol. 16, no. 9, pp. 1727–1742, May 2022, doi: 10.1049/gtd2.12389.

[24] Y. Wang, Y. Qin, Z. Ma, Y. Wang, and Y. Li, "Operation optimisation of integrated energy systems based on cooperative game with hydrogen energy storage systems," *Int. J. Hydrogen Energy*, vol. 48, no. 95, pp. 37335–37354, Dec. 2023, doi: 10.1016/j.ijhydene.2023.06.170.

[25] S. Luo, Q. Li, Y. Pu, X. Xiao, W. Chen, S. Liu, and X. Mao, "A carbon trading approach for heat-power-hydrogen integrated energy systems based on a vickrey auction strategy," *J. Energy Storage*, vol. 72, Nov. 2023, Art. no. 108613, doi: 10.1016/j.est.2023.108613.

[26] X. He, J. Jiang, and W. Hu, "Cross effects of government subsidies and corporate social responsibility on carbon emissions reductions in an omnichannel supply chain system," *Comput. Ind. Eng.*, vol. 175, Jan. 2023, Art. no. 108872, doi: 10.1016/j.cie.2022.108872.

[27] W. J. Kostowski and J. Skorek, "Real gas flow simulation in damaged distribution pipelines," *Energy*, vol. 45, no. 1, pp. 481–488, Sep. 2012, doi: 10.1016/j.energy.2012.02.076.

[28] C. Kang, T. Zhou, Q. Chen, J. Wang, Y. Sun, Q. Xia, and H. Yan, "Carbon emission flow from generation to demand: A network-based model," *IEEE Trans. Smart Grid*, vol. 6, no. 5, pp. 2386–2394, Sep. 2015, doi: 10.1109/TSG.2015.2388695.

[29] V. M. Fthenakis and H. C. Kim, "Photovoltaics: Life-cycle analyses," *Sol. Energy*, vol. 85, no. 8, pp. 1609–1628, Aug. 2011, doi: 10.1016/j.solener.2009.10.002.

[30] B. Tremeac and F. Meunier, "Life cycle analysis of 4.5 MW and 250W wind turbines," *Renew. Sustain. Energy Rev.*, vol. 13, no. 8, pp. 2104–2110, Oct. 2009, doi: 10.1016/j.rser.2009.01.001.

[31] W. Jiang, C. Liu, and Z. Sun, "Promoting developments of hydrogen production from renewable energy and hydrogen energy vehicles in China analyzing a public-private partnership cooperation scheme based on evolutionary game theory," *Energy*, vol. 278, Sep. 2023, Art. no. 127654, doi: 10.1016/j.energy.2023.127654.

[32] Z. Guo, H. Bian, C. Zhou, Q. Ren, and Y. Gao, "An electric vehicle charging load prediction model for different functional areas based on multithreaded acceleration," *J. Energy Storage*, vol. 73, Dec. 2023, Art. no. 108921, doi: 10.1016/j.est.2023.108921.

[33] H. Bian, Z. Guo, C. Zhou, X. Wang, S. Peng, and X. Zhang, "Research on orderly charge and discharge strategy of EV based on QPSO algorithm," *IEEE Access*, vol. 10, pp. 66430–66448, 2022, doi: 10.1109/ACCESS.2022.3185236.

[34] G. Zhao and E. R. Nielsen, "Environmental impact study of BIG HIT," Dept. Energy Convers. Storage, Technical Univ. Denmark, Tech. Rep. Ares(2018)4510066, 2018. [Online]. Available: https://www.bighit.eu/reports

[35] X. Xu, H. Jia, X. Jin, X. Yu, and Y. Mu, "Study on hybrid heat-gas-power flow algorithm for integrated community energy system," *Proc. CSEE*, vol. 35, no. 14, pp. 3634–3642, 2015, doi: 10.13334/j.0258-8013.pcsee.2015.14.018.

[36] Y. Zhou, X. Li, H. Han, Z. Wei, H. Zang, G. Sun, and S. Chen, "Resilience-oriented planning of integrated electricity and heat systems: A stochastic distributionally robust optimization approach," *Appl. Energy*, vol. 353, Jan. 2024, Art. no. 122053, doi: 10.1016/j.apenergy.2023.122053.

HAIHONG BIAN was born in Yancheng, China, in 1979. She received the B.S. and M.A. (Eng.) degrees from Hohai University, in 2001 and 2003, respectively, and the Ph.D. degree in electrical engineering from Southeast University.

She is currently a Professor with the School of Electrical Power Engineering, Nanjing Institute of Technology. Her research interests include power system analysis, operation, and control.

CHENGANG ZHOU was born in Yangzhou, China, in 1999. He received the B.E. degree in electrical engineering from Luoyang Institute of Science and Technology, Luoyang, China, in 2021. He is currently pursuing the M.A. (Eng.) degree with the Department of Electrical Engineering, Nanjing Institute of Technology, Nanjing, China.

His research interests include EV charging station planning, artificial intelligence algorithm, and integrated energy system planning.

ZHENGYANG GUO was born in Taizhou, in 1999. He received the B.S. and M.A. (Eng.) degrees from Nanjing Institute of Technology, Nanjing, China.

He is currently with State Grid Hangzhou Power Supply Company. His research interests include the interaction between electric vehicles and the power grid, the application of artificial intelligence and high-performance computing in the power systems, and integrated energy system planning.

YIZHOU ZHOU (Member, IEEE) received the B.S. and Ph.D. degrees in electrical engineering from Hohai University, Nanjing, China, in 2015 and 2020, respectively.

He was a Visiting Scholar with Illinois Institute of Technology, Chicago, USA, from October 2018 to October 2019. He is currently a Lecturer with the College of Energy and Electrical Engineering, Hohai University. His research interests include integrated energy systems, power system operation and planning, and electricity markets.

QUANCE REN was born in Wenzhou, in 2000. He received the B.S. degree from Jiangsu Ocean University, Lianyungang, China. He is currently pursuing the M.A. (Eng.) degree with the Department of Electrical Engineering, Nanjing Institute of Technology, Nanjing, China.

His research interests include electric vehicle charging guidance and robust optimization of electric vehicle integrated energy stations.